Modeling the binding and function of metabotropic glutamate receptors.

Xavier Rovira, David Roche, Juan Serra, Julie Kniazeff, Jean-Philippe Pin, Jesús Giraldo

Modeling the Binding and Function of Metabotropic Glutamate Receptors*

Xavier Rovira, David Roche, Juan Serra, Julie Kniazeff, Jean-Philippe Pin, and Jesús Giraldo

Grup Biomatemàtic de Recerca, Institut de Neurociències and Unitat de Bioestadística, Universitat Autònoma de Barcelona, 08193 Bellaterra, Spain (X.R., D.R., J.S., J.G.); CNRS,UMR 5203, Institut de Génomique fonctionnelle, Montpellier, France and INSERM,U661,Montpellier, France and Université Montpellier,1,2, Montpellier, France. (J.K., J.-P.P.)

RUNNING TITLE: Mathematical modeling of mGlu receptors

Corresponding author: Jesús Giraldo

Grup Biomatemàtic de Recerca, Institut de Neurociències and Unitat de Bioestadística, Universitat Autònoma de Barcelona, 08193 Bellaterra, Spain

Phone: +34 93 5813813

FAX: +34 93 5812344

E-mail address: Jesus.Giraldo@uab.es

Number of text pages: 33

Number of tables: 4

Number of figures: 7

Number of references: 30

Number of words in the Abstract: 249

Number of words in the Introduction: 522

Number of words in the Concluding Remarks: 708

ABBREVIATIONS: AM, allosteric modulator; CRD, cysteine-rich domain; GABA, gamma-aminobutyric acid; GPCR, G protein-coupled receptor; HD, heptahelical domain; mGlu, metabotropic glutamate; NAM, negative allosteric modulator; PAM, positive allosteric modulator; VFT, Venus Flytrap.

RECOMMENDED SECTION: Neuropharmacology

ABSTRACT

A mathematical model for the binding and function of metabotropic glutamate receptors was developed, with the aim to gain new insights into the functioning of these complex receptors. These receptors are homodimers and each subunit is composed of a ligand binding (VFT) domain and a heptahelical domain (HD) responsible for G-protein activation. Our mechanistic model integrates all structural information available so far: the various states of the VFT dimer (open-open, closed-open and closed-closed), as well as the fact that a single HD is active at a time. To provide the model with parameters with biological meaning, two published experimental studies were reanalyzed. The first one reports a negative cooperativity in agonist binding (Suzuki Y et al (2004) J Biol Chem 279:35526-35534) while the other indicates a positive cooperativity in agonist-mediated response (Kniazeff J et al (2004) Nat Struct Mol Biol 11:706-713). The former study allowed us to explain the mechanistic features associated with VFT recognition by agonists and antagonists integrating a negative allosteric interaction for agonist binding. The second study helped us to quantitatively describe the functional dynamics of transduction of the VFT occupation into functional response, confirming a putative positive cooperativity at the level of receptor coupling efficacy. This model will help both to better understand the functioning of these receptors and to characterize the mechanism of action of various types of allosteric modulators. Moreover, this model may be of general utility for oligomeric systems in which the ligand binding and effector domains correspond to distinct structural domains.

The two main neurotransmitters, glutamate and GABA activate not only ionotropic receptors, but also G-protein coupled receptors (GPCRs) called the metabotropic glutamate (mGlu) and $GABA_B$ receptors, respectively. These receptors belong to the class C of the large GPCR family (Pin et al., 2003), and play essential roles in the central nervous system by regulating fast excitatory and inhibitory transmission. As such, these receptors are the subject of intense research for the development of new drugs targeting the central nervous system.

In addition to their sequence divergence with the other GPCRs, mGlu and $GABA_B$ receptors have peculiar structural characteristics. These receptors form constitutive dimers that are stabilized by a disulfide bridge in the case of mGlu receptors. Moreover, each protomer of a mGlu dimer is composed of three main structural domains: an extracellular Venus Flytrap (VFT) domain where agonists bind, a transmembrane heptahelical domain (HD) responsible for G-protein activation, and a cystein-rich domain (CRD) that interconnects the VFT and the HD both structurally and functionally (Rondard et al., 2006). These structural features make these receptors complex proteins and raise several issues regarding how agonist binding in the VFT leads to G-protein activation by the HD.

Important information on the functioning of these proteins has been obtained from mutagenesis and structural studies (Galvez et al., 2000; Bessis et al., 2002; Kunishima et al., 2000; Tsuchiya et al., 2002; Bessis et al., 2000). It is now recognized that agonist binding in the VFT stabilizes the closed state of the VFT, which stabilizes in turn a new position of the VFTs relative to one another in the dimer. Such a relative movement of the VFTs has been proposed to favor a new relative position of the HDs leading to the activation of one of them (Hlavackova et al., 2005).

Mathematical models, empirical or mechanistic, have been widely used to study complex systems in biology. The former models pose the main advantage of being simple, offering, therefore, the easy determination of crucial parameters, which, although lack physical meaning, serve to characterize the general functioning properties of these systems. In contrast, mechanistic models aimed at mimicking mathematically the expected functioning of the protein complex can help to validate details of the proposed mechanism and can provide important information to better understand the mechanism of action of modulatory compounds. Indeed, not only the mGlu receptor structure is complex, but also its functional properties. For example, whereas positive cooperativity functional effect of the agonist was reported (Kniazeff et al., 2004) by analyzing the response of these dimeric receptors, a negative cooperativity between agonists binding sites was found (Suzuki et al., 2004) using binding experiments. Moreover, in addition to agonists and antagonists, a number of allosteric modulators (AM) with either positive (PAM) or negative (NAM) effects have been identified, the PAMs enhancing either agonist affinity or agonist potency or both (Goudet et al., 2004).

Here we present a mechanistic model for the ligand binding and the functioning of the dimeric mGlu receptors. This model accommodates very well both binding and functional data published on these dimeric receptors, and rationalizes the different kind of cooperativity reported for agonist binding and agonist mediated functional effects.

Methods

Modeling Concentration-Signal Curves. Empirical and mechanistic models are commonly fitted to curve data points to provide parameter estimates for comparison between either ligands or receptors. In the empirical case, the parameters lack physical meaning whereas in the mechanistic, the parameters are the chemical constants of the process. Concentration-signal curves (where signal stands for bound ligand or functional response) are normally depicted using the logarithm function for the ligand concentration, leading to sigmoid curves. In this paper, a mechanistic model was developed, which, when convenient, was handled empirically by grouping chemical constants into empirical parameters.

Curve Shape Analysis. Quantitative curve shape analysis is necessary for accurate comparisons between concentration-signal curves. The following pharmacologic descriptors can be used for the shape analysis of f(x) curves, where f stands for the signal and x=log[A], being [A] ligand concentration (Giraldo et al., 2002; Giraldo, 2003):

- The right asymptote of f as x increases: $\text{Right} = \lim_{x \to \infty} f$.
- The left asymptote of f as x decreases: $\text{Left} = \lim_{x \to -\infty} f$.
- The location of the curve or mid-point (x_{50}): x for f =Left + ½ (Right-Left). Note that we use Left and Right instead of the more common terms Bottom and Top because for inverse agonists in functional studies Right is lower than Left, and Bottom and Top would not be appropriate.

- The slope of the curve at the mid-point (x_{50}). That is, the value of the first derivative of the function at x_{50}: $\left(\frac{df}{dx}\right)_{x_{50}}$. This descriptor is directly related with the Hill coefficient at x_{50}: $n_{H_{50}} = \frac{4}{(Right - Left)\cdot \ln 10}\cdot\left(\frac{df}{dx}\right)_{x_{50}}$.
- The index of asymmetry of the curve: The distance between x_{50} and the point of inflection (x_I). The point of inflection is a point on a curve at which the curvature changes from convex to concave or vice versa. At x_I, the first derivative of the f(x) function is a maximum or minimum and, as a consequence, the second derivative is equal to zero. The location of the point of inflection serves for the assessment of the symmetry of the curve. An f(x) curve is symmetric if the point of inflection matches the mid-point, $x_I = x_{50}$, and asymmetric if it does not, $x_I \neq x_{50}$.
- The number of inflection points to distinguish between monophasic curves (one inflection point) and biphasic curves (three inflection points).
- The grade of positive or negative cooperativity of one bound ligand onto the binding of the next for a dimeric receptor: the difference between the slope at the mid-point for the concentration-signal function (f) under study and the monophasic $f = \frac{1}{1+10^{x_{50}-x}}$, where the latter presents a slope parameter of one.

The Problem of Parameter Estimation in Over-Parameterized Models: Evolutionary Algorithms versus Classical Gradient Fittings. Classical fittings by gradient nonlinear procedures pose the drawback of their dependence on initial

parameter values. These procedures are not appropriate for models where many parameters are included and many local minima are supposed to exist, as many solutions included the global minimum may be ignored. Evolutionary Algorithms (EA) (Eiben and Smith, 2003) can be used as a viable alternative to these problems. EA explore the complete parameter space by including, in a computational program, the mechanisms of reproduction, mutation and the Darwinian principles of natural selection. Mimicking biological evolution, these programs iteratively generate better and better solutions by creating new generations of parameter estimates. As EA follow stochastic rather than gradient methods, the possibility for solutions to become trapped in local minima are lower (Moles et al., 2003). Because of the considerable number of parameters involved in our mechanistic model, an in-house evolutionary algorithm (Roche et al., 2006) was used. We expect that a beta version of the program will be accessible to researchers in the near future (in the web page of some of the authors: http://servet.uab.es/biomathematics).

Statistics. Statistical comparisons between two groups (WT and mutated receptors) were performed by unpaired Student's t-test, with the inclusion of Sidàk correction for multiple comparison tests. $P<0.05$ was considered statistically significant.

Results and Discussion

Mathematical Modeling of mGlu Molecular Mechanism

Structural studies identified three states for the dimeric VFT domain: open-open (OO), closed-open (CO), and closed-closed (CC), which, if connected to the HD, give no, partial and full activity, respectively (see (Pin et al., 2004) for a review). These different states were included in our modeling schema (Figure 1). The distribution of these various states is governed by equilibrium constants according to a conformational induction approach (see Figure 1 in Supplementary material for a discussion on conformational and selection approaches). Thus, K_1 and K_2 are equilibrium dissociation constants for ligand binding to open states whereas X_i and Y_i are induction constants for the closure of open states from either free or occupied receptors, respectively. As illustrated in Fig. 1, the equilibrium between inactive and active HD dimers is governed by a constant (L) depending on the state (OO, CO, or CC) of the VFT dimer.

Following a parsimony procedure, we developed first the mathematical equations for ligand binding to the VFT domain and, then, we included the connection to the HD to achieve fully a mechanistic description of receptor function.

Modeling the Binding of Ligands to the VFT Domain

The binding of a ligand A to the VFT receptor model depicted in Figure 1 is described by Equation 1.

$$f = \frac{[A_{bound}]}{2[R_t]} = \frac{10^{x_d + x_{50} + x} + 10^{2x}}{10^{2x_{50}} + 2 \cdot 10^{x_d + x_{50} + x} + 10^{2x}} \qquad (1)$$

where $x=\log[A]$ and x_{50} (the concentration of ligand for half-occupation of the receptor binding sites) and x_d (determines the cooperativity and the shape (number of phases) of

the curves) are empirical parameters depending on the equilibrium constants included in the mechanism (see Equation A1 in the Appendix).

To analyze ligand binding, we used Equation 1 following both empirical and mechanistic approaches. Three conditions can be considered for the x_d parameter, $x_d=0$, $x_d<0$, and $x_d>0$. If $x_d=0$ then $f = \frac{1}{1+10^{x_{50}-x}}$, and the ligand binds the dimeric receptor as it would do for a monomeric receptor (absence of cooperativity and monophasic curve). The other two conditions are related with the presence of cooperativity and then the appearance of biphasic curves (see below).

To illustrate the meaning of cooperativity in terms of Equation 1, Figure 2 depicts the fractional binding for three ligands with a common x_{50} (-9) value and different x_d (0, -3, +3) values. Relative to the reference $x_d=0$ (solid line), for $x_d=-3$ a steeper curve (long dashed line) in the mid-point is obtained, indicating positive cooperativity, whereas for $x_d=+3$ a flatter curve in the mid-point is obtained, indicating negative cooperativity (short dashed line). To compare the steepness of the f(x) curves, the Hill coefficient at the mid-point ($n_{H_{50}}$) can be used (see Methods). In the simulations (see Figure 3), and using Equation A2 in the Appendix (Giraldo, 2003), values of 1, 1.998, and 0.002 were determined for $n_{H_{50}}$ with $x_d=0$, -3 and +3, respectively.

The Sign and Extent of Cooperativity and the Number of Phases of Saturation Binding curves. The value of $n_{H_{50}}$ is commonly used for cooperativity characterization, and values of 1, greater than 1 and lower than 1 are attributed to absent, positively present, and negatively present cooperativity, respectively, and this is consistent with our model (Figure 4, and paragraph above). It is worth noting that a $n_{H_{50}}$ greater than one is an indication of receptor oligomerization but values equal or

lower than one are also compatible with multiple receptor binding sites. The relationship between oligomerization and cooperativity has been discussed previously (see for instance (Park et al., 2002) for M_2 muscarinic receptors, (Strange, 2005) for D_2 dopamine receptors, (Urizar et al., 2005) for glycoprotein hormone receptors, (Vilardaga et al., 2008) for the cross-talk between α_{2A}-adrenergic and μ-opioid receptors, and (Springael et al., 2007; Milligan and Smith, 2007) for reviews). In particular, it is worth mentioning the proposal that binding experiments can be used to prove the existence of receptor dimers, suggested on the basis of experiments on vasopressin and oxytocin receptors showing positive or negative cooperativity (Albizu et al., 2006).

The steepness, measured by $n_{H_{50}}$, and the number of phases of saturation binding curves are not independent properties. As illustrated in Figure 2, for ligands showing either a neutral or a positive cooperativity a monophasic curve is obtained whereas ligands having a negative cooperativity give a biphasic curve. This observation is further confirmed by the number of inflection points on these curves (Figure 3). Whereas a single point of inflection at x=-9 (monophasic curves) for the neutral (Figure 3A) and positive cooperative (Figure 3B) ligands is observed, two additional points, at x=-5.7 and x=-12.3 (see Appendix Equation A3), are obtained for the negative cooperativity (Figure 3C) ligand.

As shown in Figure 4 however, the number of phases for ligands with negative cooperative binding can only be detected if x_d>log2 (Figure 4, red line). The relationship between x_d and $n_{H_{50}}$ (Equation A2) reveals that for negative cooperativity ($n_{H_{50}} < 1$), two phases can be detected (three inflection points) when $n_{H_{50}} < 0.67$, but not for $0.67 \leq n_{H_{50}} < 1$.

Accurate characterization of curve shapes is fundamental for the correct analysis of binding experiments. Equation 1, in its empirical form (two parameters: x_{50} and x_d), has proved instrumental for the detection of the sign and extension of cooperativity and the identification of the possible existence of two phases, in the case of negative cooperativity. It is worth noting that negative cooperativity can be accounted by other mathematical models as, for instance, the two-independent sites model or a monovalent receptor interacting with a G protein. However, positive cooperativity cannot be explained without considering the receptor as multivalent (Albizu et al., 2006; Mattera et al., 1985; Christopoulos and Kenakin, 2002; Franco et al., 2006).

Cooperativity Binding Effects and the mGlu Molecular Mechanism. After exploring in detail using an empirical approach the effects of cooperativity on the saturation binding curves, the question arises on what mechanistic determinants control this property according to the VFT binding model represented in Figure 1. As shown in the Appendix (Equation A1), the cooperativity parameter x_d was defined as $x_d = \log \frac{c_1}{2\sqrt{c_2}}$, where c_1 and c_2 depend on the equilibrium constants included in the binding mechanism. Actually, each of the cooperativity conditions can correspond to several sets of binding constants and, accordingly, there is not a unique solution to describe either positive, negative or absence of cooperativity. Nevertheless, some particular cases are worth to be discussed.

- Case 1): $K_1=K_2$, $Y_5=X_1$, $Y_6=X_2$, $Y_1=Y_2=Y_5$, $Y_3=Y_4=Y_6$; $x_d=0$, and the ligands show no cooperativity.
- Case 2): $K_1>K_2$, $Y_5=X_1$, $Y_6=X_2$, $Y_1=Y_2<Y_5$, $Y_3=Y_4<Y_6$; $x_d<0$, and the ligands show positive cooperativity.

- Case 3): $K_1<K_2$, $Y_5=X_1$, $Y_6=X_2$, $Y_1=Y_2>Y_5$, $Y_3=Y_4>Y_6$; $x_d>0$, and the ligands show negative cooperativity.

We see that absence of cooperativity can be obtained if the three horizontal branches of the VFT part in Figure 1 have the same weight; positive cooperativity, if the lowest branch (doubly occupied receptor) has higher weight than the middle branch (singly occupied receptor); and negative cooperativity, if the lowest branch has lower weight than the middle branch. The above equilibrium constants relationships are qualitatively consistent with the cooperativity concept but, to obtain a quantitative explanation of the mechanism and provide biologically meaningful parameters, an application to experimental data is needed.

Reanalyzing Experimental Binding Data with the VFT Mathematical Model. One study (Suzuki et al., 2004) examined experimentally the cooperativity between VFT binding sites upon ligand binding. The authors used the purified soluble VFT dimer of mGlu1 as a model, and four ligands (two agonists: glutamate and quisqualate and two antagonists: (S)-MCPG and LY367385) were investigated. The Hill analysis of the titration curves showed cooperativity only for glutamate (negative cooperativity). Interestingly, in the presence of calcium ions the values of x_{50} decreased for agonists but not for antagonists, indicating that the positive effects of calcium ions on receptor affinity is specific for agonist binding, and therefore is associated to the stabilization of the active (closed) conformation of the VFT protomers (both CO and CC states). In addition, the Hill coefficient of glutamate binding at the mid-point changed from 0.55 to 0.70 upon addition of calcium ions, revealing an effect on the cooperativity of glutamate binding. For quisqualate, Hill coefficients of 1.04 and 0.92 were obtained in the absence and in the presence of calcium ions, respectively, and a parallel left shift of the curve

upon addition of calcium was observed (Table 1, experimental x_{50} and $n_{H_{50}}$ values in italics).

These results can be well accommodated within our model. Table 1 shows some combinations of parameter values compatible with the above experimental findings. Although the values are arbitrary in absolute terms, the relation between them follows a plausible pharmacologic criterion, thereby allowing for a quantitative exploration of mechanistic hypotheses. Glutamate in the absence of calcium ions was taken as a reference, and the following conditions were stated: i) closure of VFT is rare in the absence of ligand ($X_1=X_2=10^{-4}$); ii) binding to OO states involves negative cooperativity ($K_2>K_1$); iii) glutamate in an open VFT does not affect the closure of the unoccupied associated partner ($Y_1=X_1$); iv) as a positive agonist, glutamate in an open VFT domain induces its closure ($Y_2=5$); v) positive cooperativity was assigned to the closure induction of an occupied VFT from the previously closed neighbor ($Y_3=10^3>Y_2$); vi) because of the same arguments, $Y_5=5$ and $Y_6=10^3$; vii) the four constants Y_1 to Y_4 are linked, and $Y_4=Y_1Y_3/Y_2=2\cdot10^{-2}$.

It is worth noting that we distinguish between two cooperativity concepts: binding cooperativity and induction cooperativity. The former involves the binding to inactive (open) states and the latter points to the induction of active (closed) states. In the context of the VFT system, we hypothesize that only a closed state can induce the closure of the associated VFT and the latter must be occupied to facilitate the process -such an hypothesis is supported experimentally (Kniazeff et al., 2004); in addition, negative binding cooperativity and positive induction cooperativity were proposed for glutamate. With the above constants, a Hill coefficient of 0.54 (using Equation A2) and an x_{50} of -5.35 were obtained (see Table 1 for these and ensuing results). These values are in agreement with the above experimental results (Suzuki et al., 2004). In the presence of

calcium ions, closed states are stabilized. Thus, Y_2, Y_3, Y_5, and Y_6 were augmented. The calculated Hill coefficient increases to 0.68 (Equation A2) and the curve shifts to the left (x_{50}=-6.05).

For quisqualate, first in the absence of calcium ions, we followed a similar rationale. We maintained the constants for the binding to open states (K_1 and K_2) as in glutamate but, due to the greater agonist capability of quisqualate, we increased the constants for induction of closed states (Y_2, Y_3, Y_5, and Y_6). The consequences on the pharmacologic curve-shape descriptors relative to glutamate were an increase of the Hill coefficient from 0.54 to 1 and a left shift of x_{50} from -5.35 to -6.1. A further increase of Y_2, Y_3, Y_5, and Y_6 constants to account for the presence of calcium ions led to a further left displacement of the curve (x_{50}=-6.44) and a lowering of the Hill coefficient (n_{H50}=0.90). We see that a concomitant increase of the induction constants for the lower (Y_5, Y_6) and middle (Y_2, Y_3) rows of the VFT model (Figure 1) can yield different results on the Hill coefficient, depending on the weight of one row relative to the other.

Finally, the behavior of an antagonist (LY367385) has been simulated by giving the same values to the binding constants for the open states (K_1=K_2=10^{-6}, absence of binding cooperativity) and low values for the constants for induction of closed states (Y_2, Y_3, Y_5, and Y_6). The parameter values yield a Hill coefficient of one and an x_{50} equal to -6. For this antagonist, increasing two orders of magnitude the values of Y_2, Y_3, Y_5, and Y_6 constants, to account for the presence of calcium ions, had no effects neither in the Hill coefficient nor in the location of the curve along the X axis.

These analyses clearly illustrate that our VFT model allowed a correct description of several experimental saturation binding curves. Such mechanistic analyses revealed important information regarding the functioning of these complex dimeric receptors. Essentially, agonists and antagonists were appropriately differentiated by their different

propensity to induce the closure of the VFT binding sites relative to the basal state. A quantitative description of cooperativity was provided, which allowed, in addition, an analysis in terms of binding and induction cooperativity concepts. This formalism may explain some striking results as, for instance, the observed negative cooperativity of some agonists, which may be interpreted as the sum of negative binding (to open states) cooperativity and positive induction (of closed states) cooperativity, being the latter the characteristic which identifies a full agonist. Yet, to properly discuss agonist behavior, the transduction of binding into functional response is needed.

Modeling the mGlu Function

Transduction of VFT binding into functional response involves the activation of the HD. Both experimental data (Hlavackova et al., 2005; Damian et al., 2006) and theoretical calculations (Filizola et al., 2006) suggest that only one HD per dimer is in the active conformation at a time This is also supported by the recent results by Bayburt et al. for the rhodopsin dimer (Bayburt et al., 2007). These authors show that indeed a single rhodopsin in a dimer can reach the active M-II state at a time. Similarly, White et al., also provide interesting data showing the asymmetrical functioning of the purified NTS1 receptor dimer (White et al., 2007). The simplest model accomplishing this finding is an asymmetric two-state dimer model consisting of two identical protomers (RR) for the inactive and two different protomers (RR*) for the active dimer state, whose relative populations are governed by an equilibrium constant, say L (Equation A5).

In mGlu receptors the G-protein activating domain, HD, and the ligand-binding VFT are linked by the CRD, allowing the functional coupling between them (Rondard et al., 2006): while agonist-induced closure of one of the VFTs is required to activate the HD,

the closure of the two VFTs is necessary for full activation. In our model, the coupling between VFT and HD dimers was defined by assuming that the equilibrium constant L depends on the state of the VFT dimer, with L_1, L_2, and L_3 for OO, OC, and CC, respectively, and where the $L_1<L_2<L_3$ relationship is expected (see Figure 1 and Equation A5). Thus, in our model, the active RR* HD is present in each of the VFT states but with a different propensity of formation. Furthermore, we did not explicitly assign the R or R* to a specific HD subunit related to the state (O or C) of its associated VFT. This is in agreement with recent findings (Brock et al., 2007) showing that VFT agonist stimulation involves an inter-subunit rearrangement resulting in the activation of either HD (cis- or trans-) with the same efficiency.

The fractional functional response (f_{R*}) is defined as the fraction of receptor concentration in the active form (meaning bearing R* state).

$$f_{R*} = \frac{\left[RR^{*}_{oo_T}\right] + \left[RR^{*}_{oc_T}\right] + \left[RR^{*}_{cc_T}\right]}{\left[RR^{*}_{oo_T}\right] + \left[RR_{oo_T}\right] + \left[RR^{*}_{oc_T}\right] + \left[RR_{oc_T}\right] + \left[RR^{*}_{cc_T}\right] + \left[RR_{cc_T}\right]} = \tag{2}$$

$$2 \cdot \frac{a_1 + a_2[A] + a_3[A]^2}{a_4 + a_5[A] + [A]^2}$$

where $\left[RR_{xy_T}\right]$ and $\left[RR^{*}_{xy_T}\right]$ stand for total receptor (VFT-CRD-HD) concentrations in inactive and active HD dimer states, respectively, and xy denotes either OO, CO or CC VFT dimer states. The mechanistic definition of the a_i parameters can be found in Appendix A6 Equation.

Assessing the Shape of Concentration-Effect curves. Quantitative characterization of the shape of the fractional response given by Equation 2 may provide useful information about the ligand-receptor interaction. Thus, using the transformation x=log[A], theoretical basal and maximum or minimum responses can be calculated as the left and right asymptotes of f_{R*}, respectively (Equation 3 and 4).

$$\text{Basal response} = \text{Left} = \lim_{x \to -\infty} f_{R*} = 2 \cdot \frac{a_1}{a_4} = \frac{1}{1 + \frac{1}{2} \cdot \frac{1 + 2X_1 + X_1X_2}{L_1 + 2L_2X_1 + L_3X_1X_2}} \tag{3}$$

$$\text{Maximum or minimum response} = \text{Right} = \lim_{x \to +\infty} f_{R*} = 2 \cdot a_3 = \frac{1}{1 + \frac{1}{2} \cdot \frac{1 + 2Y_5 + Y_5Y_6}{L_1 + 2L_2Y_5 + L_3Y_5Y_6}} \tag{4}$$

The expressions for basal and maximum or minimum responses make sense as none of ligand-dependent equilibrium constants appear in the basal response whereas only constants for induction of active closed states for the doubly occupied receptor (Y_5, Y_6) appear in the maximum or minimum responses. It is worth mentioning that none of the constants involving the singly occupied receptor dimer appears in the expression for the right asymptote in agreement with an occupation of all receptor sites as [A] increases infinitely. Equations 3 and 4 measure the efficacy of the system in the absence and in the presence of the ligand, respectively (note the formal similarity between both equations). If we assume that the coupling constants L_i are not ligand-dependent, Y_5, Y_6 are the only constants responsible for the intrinsic efficacy of a ligand. A definition of

neutral antagonism, positive agonism and inverse agonism can be obtained by a comparison between basal and maximum (or minimum) responses: Right=Left, Right=maximum>basal, and Right=minimum<basal, respectively. Note that for an inverse agonist the term maximum changes to minimum. A neutral antagonist results by making $Y_5=X_1$ and $Y_6=X_2$; a positive agonist, by making $Y_5>X_1$ and/or $Y_6>X_2$; and an inverse agonist, by making $Y_5<X_1$ and/or $Y_6<X_2$. For illustration, Table 2 shows some combinations of parameters yielding to either positive or inverse agonism.

The middle row of the VFT binding part on Figure 1 (the induction of active closed states from single receptor occupation), which is not present in the definition of efficacy (maximum or minimum response - basal response), affects the potency (A_{50}) of the agonist (Appendix Equation A9). Agonist potency can be investigated for any ligand different from a neutral antagonist, where the left and right asymptotes take the same value (the denominator of Equation A9 is 0) and A_{50} is indeterminate. The ± sign in Equation A9 results for the possibility of A being either a positive or an inverse agonist. A systematic variation on the equilibrium constants included in the fractional response (Equation 2) can be found in the Supplementary Material (Figure 2). The collection of curves on display offers a mechanistic explanation for a broad range of concentration-effect profiles, including full and partial agonism, inverse agonism, monophasic, biphasic, and bell-shaped curves.

Reanalyzing Experimental Functional Data with the mGlu Mathematical Model. In the binding section of this study, experimental data were reanalyzed to encompass the theoretical pharmacological space within realistic limits. The same rationale is followed here and a recent experimental work (Kniazeff et al., 2004) involving functional studies in a full length (mG5C1-mG5C2) receptor using quisqualate as agonist was selected. In

this study, the authors observed that mutating the VFT in the binding site (the so-called YADA mutant) led to a loss of agonist-induced activity of the receptor. However, when a single VFT was mutated in the dimer (the so-called mG5C1-mG5C2-YADA mutant), agonist binding in the WT VFT allowed agonist interaction in the mutated VFT to further increase receptor activity. The resulting dose-response curve was biphasic, and two x_{50} values (x_{50_1} and x_{50_2} for the first and second phase, respectively) were identified. The x_{50_1} of quisqualate for the YADA heterodimer was close to that measured on the wild-type receptor whereas the second response yielded a maximum of ~80% of that measured with the control receptor. Similar biphasic shapes were obtained when performing some other mutations (the so-called YATA or SATA mutants). Interestingly, the x_{50_1} of quisqualate did not depend on the mutants used, while, in contrast, the x_{50_2} largely varied among the mutants. Altogether, these results suggested that mutations damage the mechanism of agonist-induced closure of the mutated protomer, and that the mechanism can be, albeit only in part, recovered by the activation of the associated WT subunit, with the first phase of the response curve resulting from agonist binding in the wild-type subunit only (Kniazeff et al., 2004).

Figure 5 shows the experimental data for WT (Figure 5A) and single-mutated VFT (Figure 5C) as solid circles. The Empirical Models 5 (Hill equation) and 6 (sum-of-two fractional Hill equations) were fitted to the former (Figure 5A, solid line) and the latter (Figure 5C, solid line) receptor systems, respectively.

$$f = \text{Basal} + \frac{\text{Maximum} - \text{Basal}}{1 + 10^{n_H (x_{50} - x)}} \qquad (5)$$

$$f = \text{Basal} + \frac{(\text{Maximum} - \text{Basal}) \cdot p}{1 + 10^{n_{H1}(x_{50_1} - x)}} + \frac{(\text{Maximum} - \text{Basal}) \cdot (1 - p)}{1 + 10^{n_{H2}(x_{50_2} - x)}} \qquad (6)$$

For the WT VFT (Figure 5A), the parameter estimates under Equation 5 were: Basal=0.46, Maximum=0.99, $x_{50} = -7.24$, and n_H=1.26 (see Table 3 for these and ensuing results). It is worth mentioning the unusual very high value found for the basal response in this experiment, being the typical ones around 20-25% of the maximal response. The value -greater than one- for the Hill coefficient (n_H) suggests that positive cooperativity is originally present in the WT receptor if quisqualate is used as agonist. For the single-mutated VFT, the parameter estimates under Equation 6 were Basal=0.41, Maximum=0.89, p=0.30, $x_{50_1} = -6.93$, $n_{H_1} = 1.33$, $x_{50_2} = -3.56$, and $n_{H_2} = 1.09$. After mutation, a decrease in the maximum response and a split of the curve into two phases are observed (Figure 5C). As shown earlier (Kniazeff et al., 2004), the value for x_{50_1} is close to that measured on the WT receptor. Interestingly, this similarity is also observed for n_{H_1}. Both properties indicate that the first response comes from quisqualate binding in the wild-type subunit only and that the response-generating machinery for the WT protomer is not significantly affected by mutation. As mentioned above, a demonstration for this comes from the different x_{50_2} values and a common x_{50_1} value obtained with different mutants (see Fig 5d of Kniazeff et al 2004). Finally, the decrease of both the maximum response and the second Hill coefficient suggests that the functional activity provided by the mutated protomer is partially reduced.

To provide a mechanistic interpretation of the experimental data, the WT curve was examined using the model developed for mGlu function (Equation 2). The high number

of parameters included in the equation and the correlation likely existing between them preclude the use of classical gradient non-linear fittings. Accordingly, a stochastic evolutionary algorithm was used (see Methods). To do this, we chose first a reference state by taking the values listed in Table 1 for the quisqualate-VFT interaction in the absence of calcium together with plausible values for the VFT-HD allosteric constants (basically, the $L_1<L_2<L_3$ relationship). To assure sufficient sampling of parameter population, a ±3 interval was chosen for each optimized parameter and 100 independent runs were performed. Table 3 shows the mean and standard deviations of each of the parameters. Essentially, we found negative cooperativity for the binding to the OO sites ($K_1<K_2$), positive cooperativity for the induction of closed states both in singly ($Y_2<Y_3$) and in doubly ($Y_5<Y_6$) occupied VFT dimers, and the expected $L_1<L_2<L_3$ relationship for the transduction of occupation into response. Figure 5B shows the theoretical curve produced by that run out of 100 whose parameters are closest (Euclidean distance) to the mean values. Visual comparison with the curve produced by the empirical one-site model (Figure 5A) indicates a similar fitting which is confirmed by the x_{50} and $n_{H_{50}}$ curve-shape descriptors (Table 3).

For the mutated VFT, we used the values inferred for the WT receptor as a starting point, and our evolutionary algorithm was employed to obtain the optimized parameters. For simplicity, we considered first that only some of the constants -those directly associated with the mutated protomer- could change after mutation; that is, K_2, Y_3, and Y_6. Furthermore, because the mutation of the VFT of one protomer may alter the ability of the dimer to transmit the signal, L_1, L_2, and L_3 were allowed to change as well. A systematic analysis was performed to identify the equilibrium constants mainly affected by the mutation: successive independent fittings were carried out ranging from a single optimized parameter to all possible combinations of parameters (that is, from 2 to 6

optimized parameters). In all cases, a ±3 interval was allowed for each of the parameters varied. Interestingly, when only one optimized parameter was contemplated in the fitting, three of them clearly differentiated from the others in the capacity of reducing the sum of squares of the error: L_3, Y_6, and K_2, in decreasing order. Moreover, the combinations of two parameters leading to best fittings were (L_3,K_2), (L_3,Y_6), and (K_2,Y_6).

These results indicate that the main effects of VFT mutation on functional response are: (i) an impairment of the allosteric VFT-HD interaction associated to the CC state (L_3), (ii) a diminution of the capacity of the first closed protomer (supposedly the WT) to induce the closing of the second protomer (supposedly the mutated) in the doubly occupied VFT (Y_6), and (iii) a decrease in the affinity of the ligand for the second binding site (K_2).

To test statistically the above hypotheses on parameter modification after receptor mutation, 100 independent runs were performed for the mutated receptor, with all fit parameters free and a ± 3 interval for each of the parameters (Table 3). Statistical comparison between WT and mutated receptor by Student's t-test, including Sidàk correction for multiple comparisons, confirmed the mechanistic proposals suggested above. As expected, changes on K_2, Y_6, and L_3 reached statistical significance. The other parameters that significantly changed on receptor mutation were L_1, Y_2, X_1, and X_2. As it can be seen from Equation 3, $L_1 \approx Basal/(2(1-Basal))$ if X_1 and X_2 are much lower than 1. Then, the change on L_1 reflects the observed change on the basal response. The model predicts a half lowering of Y_2 after mutation, which suggests that the mutant protomer hampers the closing of the occupied WT. This indicates that a mutation on the recognition site of one protomer affects the binding and activation capacity of the mutated unit but also the intrinsic efficacy of the WT partner. The lower values for X_1

and X_2 on the mutated relative to the WT receptor are consistent with above findings. Finally, to illustrate the goodness of fitting of our mechanistic approach, Figure 5D shows the theoretical curve produced by that run out of 100 for which the parameters are the closest (Euclidean distance) to the mean values. The apparent resemblance with the fitting produced by the empirical two-sites model (Figure 5C) is quantitatively confirmed by the location and Hill coefficients parameters (Table 3). However, only the mechanistic model provides a detailed view of the important steps of the activating process affected by the mutations.

Functional Dynamics of WT and Mutated Receptors: The Distribution of VFT States upon Ligand Binding. Figure 6s shows the relative distribution of VFT states for both WT and mutated receptors (Kniazeff et al., 2004) using the same mechanistic constants values as in Figures 5B and 5D. We see that WT and mutated receptor profiles show similarities and differences. The maximum asymptote as [A] decreases (on the left) corresponds to the free open (OO) state (solid red line). The fractional concentration of this state ranges between 1 and 0, reaching the asymptotic minimum value for lower [A] values in the case of the WT. Two bell curves appear in both cases, which correspond to singly occupied O_AO (long-dashed red line) and C_AO (long-dashed blue line) VFT states. These curves are broader for the mutated receptor indicating that the importance of these states spans over a longer [A] range for this receptor genotype. Interestingly, the O_AO state, which is slightly present in the WT, contributes significantly to the VFT distribution in the mutated receptor. The maximum asymptotes as [A] increases (on the right) correspond to doubly occupied states. However, whereas in the case of the WT all the doubly occupied receptors are in the fully active C_AC_A form (short-dashed green line), a distribution of states are obtained for the mutated

receptor, namely, fractional 0.75, 0.20 and 0.05 values for the fully active C_AC_A (short-dashed green line), partially active O_AC_A (short-dashed blue line), and slightly active O_AO_A (short-dashed red line), respectively, are found. In addition, the significant presence of C_AC_A starts at lower concentrations for the WT. Comparison between Figures 6B and 5D shows that the functional intermediate plateau of the mutated receptor is produced mainly by the C_AO state as it is both more abundant and more efficacious (L_2>L_1) than the O_AO state. Figure 6B helps understand the functional dynamics of mutated receptor. Basal response is due to OO state; accumulative addition of A leads first to single occupation, which can be in either O_AO and C_AO forms, where mainly the WT protomer is occupied in the singly occupied mutated receptor -the relevant importance of the O_AO species compared to the WT receptor is an indication that mutation of a protomer affects also the propensity of closure of the WT partner; increasing further [A] leads to doubly occupied receptors in the order [C_AC_A] > [O_AC_A] > [O_AO_A], being the two latter states concentrations non-negligible in contrast to the WT receptor.

The Cooperativity Issue and the Ligand Recognition Mechanism: The application of the model to structure-activity studies

(The model cannot help identifying ligand with a specific structure, but rather be usefull in predicting the existence of ligand with specific properties. This point was not well understood by one referee likely because of the term "structure-activity". I suggest you change this title.)

As quantitatively shown above, the combination of two states (open and closed) and domain dimerization provides the receptor with a flexible mechanism for ligand

recognition and signal transduction. In the present article two conceptually different cooperativity classes for the mGlu receptor have been proposed, binding and induction, the former related with binding to inactive VFT open states and the latter related to induction of active VFT closed states. The model presented herein suggests that, if we assume three categories, absent (0), positive (+), and negative (-), for both binding and induction cooperativities, nine types of ligands could, in principle, exist from the {binding, induction} combination of cooperativities. One of the combinations {-,+} was identified for glutamate and quisqualate full agonists (Table 1). The sign of the cooperativities indicates that whereas the binding of the first ligand to the OO state diminishes the binding of the second ligand to the same state (negative binding cooperativity), the closure of a VFT protomer facilitates the closure of the second (positive induction cooperativity). Interestingly, other combinations, as for instance {+,-}, are theoretically possible and would yield to a potent partial agonist, i.e. a ligand with lower maximum response but a significantly left-shifted functional curve relative to a more efficacious full agonist. Figure 7 displays the concentration-effect curves of two agonists with opposite cooperativity effects. One agonist (solid curve) poses negative binding cooperativity **($K_1=10^{-5}$, $K_2=10^{-3}$)** and positive induction cooperativity **($Y_2=Y_5=10$, $Y_3=Y_6=10^{2}$)**, the other agonist (dashed curve), on the contrary, bears positive binding cooperativity **($K_1=10^{-5}$, $K_2=10^{-7}$)** and negative induction cooperativity **($Y_2=Y_5=10$, $Y_3=Y_6=10^{-2}$)**. Comparison of the curves shows a **slight** left-shift displacement including an increase of the slope and a **notable** decrease of the maximum response of the latter curve relative to the former one, converting a full agonist into a partial but **not less** potent **(in the common response range)** agonist. Structure-activity studies identified the so-called APTC, a new family of mGlu orthosteric ligands (Schann et al., 2006). Amongst the series of synthesized ligands, one (FP0429) was

shown to be a full mGlu4 agonist and a partial mGlu8 agonist. As these receptors are highly homologous, the question on the structural features responsible for ligand specific properties arose. Site-directed mutagenesis of two residues within the binding site that differ between mGlu4 and mGlu8 switched the agonist definition of FP0429 from full to partial agonist and vice versa (Frauli et al., 2007). Interestingly, docking analysis in mGlu VFT model attributed a role in agonist binding to one of the residues while the other participated in the closure, thus the functional activity (Frauli et al., 2007). This explanation is consistent with our conceptual distinction between binding and functional (induction) cooperativities, suggesting that approaches based on the cooperativity issue may be of interest in the drug discovery process. **To this end and with the aim of helping chemists in their structure-activity analysis, Table 4 shows the association of the mechanistic parameters of the model (the equilibrium constants of Fig 1) with the typical pharmacological properties basal response, efficacy, potency, and slope.**

Concluding Remarks

In the present study, a mathematical modeling of mGlu binding and function was made by constructing two models, one for the VFT and the other for the HD dimer domains. For simplicity, the analysis of ligand binding to VFT orthosteric sites was conducted without the inclusion of HD. A detailed exam of the shape of saturation binding curves in terms of the structure of the VFT lobes was performed, allowing the differentiation between positive and negative cooperativity and the description of biphasic curves. For the analysis of mGlu function, a coupling constant L, which embodies the probability of yielding an active HD dimer, was included. This constant modulates the population of active HDs upon selective binding to VFT states. According to experimental data, only one HD is activated at a time within a dimer. Thus, R*R* was precluded, and an asymmetric two-state dimer model ($RR \overset{L}{\leftrightarrow} RR^*$) was proposed.

The model allowed for the quantification of agonist efficacy and potency, and the interpretation of pharmacologic curve profiles in mechanistic terms. In addition to theoretical simulations (Supplementary Material), two published experiments, one involving binding (Suzuki et al., 2004) and the other functional (Kniazeff et al., 2004), were satisfactorily reanalyzed. An important outcome of the analysis was the mechanistic distinction between binding and induction cooperativities, the former related to the affinity of the second ligand to the OO state with respect to the binding of the first molecule and the latter to the induction of closure of the second protomer after closing of the first one. The reanalysis of the binding study (Suzuki et al., 2004) provided evidence that full agonists are characterized by positive induction (of closed states) cooperativity which, depending on the sign and magnitude of the binding (to open states) cooperativity, may lead to observed negative, null or positive cooperativity.

The reanalysis of the functional study (Kniazeff et al., 2004) identified the binding/transduction parameters that were mainly affected by receptor mutation and the different functional dynamics (VFT states distribution) of WT and mutated receptors upon agonist concentration. Moreover, based on the conceptual distinction between binding and induction cooperativities, the functional profile of a theoretically potent partial agonist was obtained, which suggests a possible application of the model in structure-activity studies.

The model also quantitatively illustrates some of the advantages for a receptor of being a dimer. A receptor failure which would make a receptor fully inactive in the case of a monomer receptor can be partially compensated by an associate protomer in the case of a dimer receptor (Kniazeff et al., 2004). In addition, the interdependence between binding sites makes a dimer receptor more efficient than the sum of two single monomers. First, positive induction cooperativity facilitates the closure of the second site, increasing the efficiency of the system. Second, negative binding cooperativity for slightly active open sites (OO) biases the receptor sites distribution towards partially active (CO) and fully active (CC) receptor sites.

It has been suggested that, in addition to the conformation of each HD within the dimer, the relative positioning between the heptahelical protomers plays an important role in signal transduction. Thus, at least two conformations for the active RR* dimeric state, $(RR^*)_a$ and $(RR^*)_b$, with a probability of occurrence depending on the VFT state are conceivable. This variety of active conformations could explain the multiplicity of pathways associated to VFT activation. It has been found that only CC leads to full activation of Gq, whereas the CO state leads both to Gs coupling and to partial Gq activation (Tateyama and Kubo, 2006; Kniazeff et al., 2004). This level of detail, which might be useful in biochemical experiments involving more than one G protein, has not

been considered necessary for the purposes of the present study, where only one conformation for the RR* active state was included.

It is remarkable that by taking an agonist as a reference, a partial but potent virtual agonist was devised by our model by inverting the binding and induction cooperativities of the reference ligand. In this regard, we expect that the mechanistic components included in the model may help chemists in their structure-activity studies to quantify the effects of drugs. A paradigmatic related example can be found in the discovery of burimamide (Black et al., 1972), the first H_2 receptor antagonist, which was obtained by taking the structure of the endogenous agonist histamine as the chemical starting point and progressively removing its agonist properties along a structure-activity pathway including partial agonists as signposts.

The inclusion in the model of VFT and HD **domains** leaves the model ready for the analysis of allosteric compounds, which, by binding to the HD, modulate the binding and/or function of orthosteric compounds acting on the VFT domain. In this regard, we expect the model to be able to account for the effects of PAMs and NAMs on constitutive activity, agonist efficacy, agonist affinity, etcetera. Moreover, a quantitative explanation of the functional differences between Ca2+ and Gd3+ on these receptors represents another challenge to the model. The analysis of experiments involving these and other molecular interventions **as, for instance, the molecular design of antagonists and inverse agonists by altering the cooperativity properties as suggested above,** will allow not only check the validity of the model but open new possibilities to tune its parameters. This will be the subject of further work.

Finally, the results suggest that our model, initially conceived for mGlu receptors, may apply to any other receptor system composed of an extracellular agonist binding domain and a transmembrane functional domain.

APPENDIX

The Fractional Binding Function for the VFT Domain

$$f = \frac{[A_{bound}]}{2[R_t]} = \frac{1}{2}\cdot\frac{c_1[A]+2[A]^2}{c_2+c_1[A]+[A]^2} = \frac{1}{2}\cdot\frac{10^{x_{c1}+x}+2\cdot 10^{2x}}{10^{x_{c2}}+10^{x_{c1}+x}+10^{2x}} = \frac{10^{x_d+x_{50}+x}+10^{2x}}{10^{2x_{50}}+2\cdot 10^{x_d+x_{50}+x}+10^{2x}} \quad \text{(A1)}$$

where the total concentration of receptors, $[R_t]$, and the concentration of bound ligand, $[A_{bound}]$, are defined as

$$[R_t]=[OO]+[O_AO]+[O_AO_A]+[OC]+[C_AO]+[O_AC]+[O_AC_A]+[CC]+[C_AC]+[C_AC_A]$$

$$[A_{bound}]=[O_AO]+2[O_AO_A]+[C_AO]+[O_AC]+2[O_AC_A]+[C_AC]+2[C_AC_A]$$

$c_1 = \frac{2K_2(1+Y_1+Y_2+Y_1Y_3)}{1+2Y_5+Y_5Y_6}$, $c_2 = \frac{K_1K_2(1+2X_1+X_1X_2)}{1+2Y_5+Y_5Y_6}$, x=log[A],

$x_{c_1} = \log c_1$, $x_{c_2} = \log c_2$, $x_{50} = \frac{x_{c_2}}{2} = x$ for f=1/2, and

$x_d = \log\frac{c_1}{2\sqrt{c_2}} = x_{c_1} - \frac{1}{2}x_{c_2} - \log 2$.

As the f binding function was defined relative to the total number of binding sites ($2[R_t]$), f ranges between 0 and 1. It is worth noting that Equation A1, expressed as a function of c_1 and c_2 parameters, is the same as that obtained for the so-called two-state dimer model (Franco et al., 2006) and, for this reason, the x_d parameter is related with a cooperativity index as empirically defined in the previous model (Casadó et al., 2007). However, the definition of the parameters is different here because, in the present

model, the states of the protomers (either closed or open) within the dimer molecule can be distinguished.

The Hill Coefficient at the Mid-Point

The Hill Coefficient at the Mid-Point, n_{H50}, is related with the first derivative at the Mid-Point, $\left(\frac{df}{dx}\right)_{x_{50}}$, by

$$n_{H50} = \frac{4}{\ln 10} \cdot \left(\frac{df}{dx}\right)_{x_{50}} = \frac{2}{1+10^{x_d}} \qquad \text{(A2)}$$

(see Methods).

Determining the Number of Phases of Sigmoid Curves

The number of phases of a sigmoid curve depends on the number of points of inflection. Monophasic curves show one point of inflection whereas biphasic curves present three. Mathematical analysis of Equation A1 shows that, in general, the number of points of inflection depend on the value of x_d relative to log 2. For $x_d \leq \log 2$, there is one point of inflection at $x=x_{50}$; for $x_d > \log 2$, there are three points of inflection, one at $x=x_{50}$ and the other two at

$$x = x_{50} - x_d + \log\left(10^{2x_d} - 2 \pm \sqrt{\left(10^{2x_d} - 2\right)^2 - 10^{2x_d}}\right) \qquad \text{(A3)}$$

The Asymmetric HD Activation Model

Equation A4 shows the equilibrium between inactive (RR) and active (RR*) HDs.

$$RR \overset{2L}{\leftrightarrow} RR^{*} \qquad \text{(A4)}$$

where R and R* stand for the inactive and active HDs within the dimer, respectively, and $2L = \frac{[RR^{*}]}{[RR]}$ is the macroscopic equilibrium constant for the equilibrium between HD dimer states.

In our model, it was assumed that the equilibrium constant L depends on the state of the VFT domain. Thus, three apparent constants for the equilibrium between inactive (RR) and active (RR*) HDs are defined:

$$2L_1 = \frac{[RR^{*}_{oo_T}]}{[RR_{oo_T}]}, \quad 2L_2 = \frac{[RR^{*}_{oc_T}]}{[RR_{oc_T}]}, \quad 2L_3 = \frac{[RR^{*}_{cc_T}]}{[RR_{cc_T}]} \qquad \text{(A5)}$$

where $\left\{\left[RR^{*}_{oo_T}\right], \left[RR^{*}_{oc_T}\right], \text{and } \left[RR^{*}_{cc_T}\right]\right\}$ and $\left\{\left[RR_{oo_T}\right], \left[RR_{oc_T}\right], \text{and } \left[RR_{cc_T}\right]\right\}$ stand for total active and inactive HD connected to open-open (OO), open-closed (OC), and closed-closed (CC) VFT, respectively.

The fractional functional response

The fractional functional response ($f_{R^{*}}$) is defined as the fraction of receptor concentration in the active form.

$$f_{R^*} = \frac{[RR^*_{oo_T}] + [RR^*_{oc_T}] + [RR^*_{cc_T}]}{[RR^*_{oo_T}] + [RR_{oo_T}] + [RR^*_{oc_T}] + [RR_{oc_T}] + [RR^*_{cc_T}] + [RR_{cc_T}]} = \tag{A6}$$

$$2 \cdot \frac{c_1 + c_2[A] + c_3[A]^2}{c_4 + c_5[A] + c_6[A]^2} = 2 \cdot \frac{a_1 + a_2[A] + a_3[A]^2}{a_4 + a_5[A] + [A]^2}$$

where

$$c_1 = K_1K_2(L_1 + 2L_2X_1 + L_3X_1X_2)$$
$$c_2 = 2K_2(L_1 + L_2(Y_1 + Y_2) + L_3Y_2Y_4)$$
$$c_3 = L_1 + 2L_2Y_5 + L_3Y_5Y_6$$
$$c_4 = K_1K_2(2L_1 + 1 + 2(2L_2 + 1)X_1 + (2L_3 + 1)X_1X_2)$$
$$c_5 = 2K_2(2L_1 + 1 + (2L_2 + 1)(Y_1 + Y_2) + (2L_3 + 1)Y_2Y_4)$$
$$c_6 = 2L_1 + 1 + 2(2L_2 + 1)Y_5 + (2L_3 + 1)Y_5Y_6;$$

and $a_i = \frac{c_i}{c_6}$ for i = 1 to 6

using the equilibrium constants depicted in Figure 1 and Equations A4 and A5.

Pharmacological Descriptors of Functional Response Curves

Using the transformation x=log[A], the theoretical basal response is calculated as the left asymptote of f_{R^*}, and the theoretical maximum or minimum response is obtained as the right asymptote of f_{R^*}.

$$\text{Basal response} = \text{Left} = \lim_{x \to -\infty} f_{R^*} = 2 \cdot \frac{a_1}{a_4} = \frac{1}{1 + \frac{1}{2} \cdot \frac{1 + 2X_1 + X_1X_2}{\alpha_1 + 2\alpha_2X_1 + \alpha_3X_1X_2}} \tag{A7}$$

$$\text{Maximum or minimum response} = \text{Right} = \lim_{x \to +\infty} f_{R^*} = 2 \cdot a_3 = \frac{1}{1 + \frac{1}{2} \cdot \frac{1 + 2Y_5 + Y_5Y_6}{\alpha_1 + 2\alpha_2Y_5 + \alpha_3Y_5Y_6}}$$

(A8)

The potency (A_{50}) of the agonist is calculated as [A] for $\text{Response} = \text{Left} + \frac{\text{Right} - \text{Left}}{2}$ (Equation A9).

$$A_{50} = \frac{-b \pm \sqrt{b^2 - 4ac}}{2a} \qquad \text{(A9)}$$

where $a = a_1 - a_3 a_4$; $b = a_3 a_4 a_5 - 2a_2 a_4 + a_1 a_5$; and $c = -a_4(a_1 - a_3 a_4)$, and the ± sign in Equation A9 results for the possibility of A being either a positive or an inverse agonist.

The sensitivity of the receptor to an increment in the agonist concentration is measured by the first derivative of the receptor function (Equation A10).

$$\frac{df_{R*}}{dx} = \frac{2\left(-\left(a_1 + a_2 10^x + a_3 10^{2x}\right)\left(a_5 10^x + 2\cdot 10^{2x}\right) + \left(2a_3 10^{2x} + a_2 10^x\right)\left(a_4 + a_5 10^x + 10^{2x}\right)\right)\ln 10}{\left(a_4 + a_5 10^x + 10^{2x}\right)^2} \qquad \text{(A10)}$$

The Hill coefficient at the midpoint $\left(n_{H_{50}} = \frac{4}{(\text{Right} - \text{Left})\cdot \ln 10} \cdot \left(\frac{df_{R*}}{dx}\right)_{x_{50}}\right)$ can be calculated from Equation A10 (Giraldo et al., 2002; Giraldo, 2003).

Acknowledgements

We thank Anna Castellano for technical assistance.

References

Albizu L, Balestre MN, Breton C, Pin JP, Manning M, Mouillac B, Barberis C, and Durroux T (2006) Probing the existence of G protein-coupled receptor dimers by positive and negative ligand-dependent cooperative binding. *Mol Pharmacol* **70**:1783-1791.

Bayburt TH, Leitz AJ, Xie G, Oprian DD, and Sligar SG (2007) Transducin activation by nanoscale lipid bilayers containing one and two rhodopsins. *J Biol Chem* **282**:14875-14881.

Bessis AS, Bertrand HO, Galvez T, de Colle C, Pin JP, and Acher F (2000) Three-dimensional model of the extracellular domain of the type 4a metabotropic glutamate receptor: new insights into the activation process. *Protein Sci* **9**:2200-2209.

Bessis AS, Rondard P, Gaven F, Brabet I, Triballeau N, Prezeau L, Acher F, and Pin JP (2002) Closure of the Venus flytrap module of mGlu8 receptor and the activation process: Insights from mutations converting antagonists into agonists. *Proc Natl Acad Sci U S A* **99**:11097-11102.

Black JW, Duncan WA, Durant CJ, Ganellin CR, and Parsons EM (1972) Definition and antagonism of histamine H 2 -receptors. *Nature* **236**:385-390.

Brock C, Oueslati N, Soler S, Boudier L, Rondard P, and Pin JP (2007) Activation of a dimeric metabotropic glutamate receptor by inter-subunit rearrangement. *J Biol Chem* **282**:33000-33008.

Casadó V, Cortés A, Ciruela F, Mallol J, Ferré S, Lluis C, Canela EI, and Franco R (2007) Old and new ways to calculate the affinity of agonists and antagonists interacting with G-protein-coupled monomeric and dimeric receptors: The receptor-dimer cooperativity index. *Pharmacol & Ther* **116**:343-354.

Christopoulos A and Kenakin T (2002) G protein-coupled receptor allosterism and complexing. *Pharmacol Rev* **54**:323-374.

Damian M, Martin A, Mesnier D, Pin JP, and Baneres JL (2006) Asymmetric conformational changes in a GPCR dimer controlled by G-proteins. *EMBO J* **25**:5693-5702.

Eiben AE and Smith JE (2003) *Introduction to evolutionary computing*. Springer-Verlag, Berlin.

Filizola M, Wang SX, and Weinstein H (2006) Dynamic models of G-protein coupled receptor dimers: indications of asymmetry in the rhodopsin dimer from molecular dynamics simulations in a POPC bilayer. *J Comput Aided Mol Des* **20**:405-416.

Franco R, Casadó V, Mallol J, Ferrada C, Ferré S, Fuxe K, Cortés A, Ciruela F, Lluis C, and Canela EI (2006) The two-state dimer receptor model: a general model for receptor dimers. *Mol Pharmacol* **69**:1905-1912.

Frauli M, Hubert N, Schann S, Triballeau N, Bertrand HO, Acher F, Neuville P, Pin JP, and Prezeau L (2007) Amino-pyrrolidine tricarboxylic acids give new insight into group III metabotropic glutamate receptor activation mechanism. *Mol Pharmacol* **71**:704-712.

Galvez T, Prezeau L, Milioti G, Franek M, Joly C, Froestl W, Bettler B, Bertrand HO, Blahos J, and Pin JP (2000) Mapping the agonist-binding site of GABAB type 1 subunit sheds light on the activation process of GABAB receptors. *J Biol Chem* **275**:41166-41174.

Giraldo J (2003) Empirical models and Hill coefficients. *Trends Pharmacol Sci* **24**:63-65.

Giraldo J, Vivas NM, Vila E, and Badia A (2002) Assessing the (a)symmetry of concentration-effect curves: empirical versus mechanistic models. *Pharmacol & Ther* **95**:21-45.

Goudet C, Binet V, Prezeau L, and Pin JP (2004) Allosteric modulators of class-C G-protein coupled open new possibilities for therapeutic application. *Drug Discov Today* **1**:125-133.

Hlavackova V, Goudet C, Kniazeff J, Zikova A, Maurel D, Vol C, Trojanova J, Prezeau L, Pin JP, and Blahos J (2005) Evidence for a single heptahelical domain being turned on upon activation of a dimeric GPCR. *EMBO J* **24**:499-509.

Kniazeff J, Bessis AS, Maurel D, Ansanay H, Prezeau L, and Pin JP (2004) Closed state of both binding domains of homodimeric mGlu receptors is required for full activity. *Nat Struct Mol Biol* **11**:706-713.

Kunishima N, Shimada Y, Tsuji Y, Sato T, Yamamoto M, Kumasaka T, Nakanishi S, Jingami H, and Morikawa K (2000) Structural basis of glutamate recognition by a dimeric metabotropic glutamate receptor. *Nature* **407**:971-977.

Mattera R, Pitts BJ, Entman ML, and Birnbaumer L (1985) Guanine nucleotide regulation of a mammalian myocardial muscarinic receptor system. Evidence for homo- and heterotropic cooperativity in ligand binding analyzed by computer-assisted curve fitting. *J Biol Chem* **260**:7410-7421.

Milligan G and Smith NJ (2007) Allosteric modulation of heterodimeric G-protein-coupled receptors. *Trends Pharmacol Sci* **28**:615-620.

Moles CG, Mendes P, and Banga JR (2003) Parameter estimation in biochemical pathways: a comparison of global optimization methods. *Genome Res* **13**:2467-2474.

Park PS, Sum CS, Pawagi AB, and Wells JW (2002) Cooperativity and oligomeric status of cardiac muscarinic cholinergic receptors. *Biochemistry* **41**:5588-5604.

Pin JP, Galvez T, and Prezeau L (2003) Evolution, structure, and activation mechanism of family 3/C G-protein-coupled receptors. *Pharmacol Ther* **98**:325-354.

Pin JP, Kniazeff J, Goudet C, Bessis AS, Liu J, Galvez T, Acher F, Rondard P, and Prezeau L (2004) The activation mechanism of class-C G-protein coupled receptors. *Biol Cell* **96**:335-342.

Roche D, Serra J, Rovira X, and Giraldo J (2006) A genetic algorithm for curve fitting: a possible choice for unsatisfactory nonlinear regressions. *Proceedings of the British Pharmacological Society* **at** **http://www.pA2online.org/abstracts/Vol4Issue2abst008P.pdf**.

Rondard P, Liu J, Huang S, Malhaire F, Vol C, Pinault A, Labesse G, and Pin JP (2006) Coupling of agonist binding to effector domain activation in metabotropic glutamate-like receptors. *J Biol Chem* **281**:24653-24661.

Schann S, Menet C, Arvault P, Mercier G, Frauli M, Mayer S, Hubert N, Triballeau N, Bertrand HO, Acher F, and Neuville P (2006) Design and synthesis of APTCs (aminopyrrolidinetricarboxylic acids): identification of a new group III metabotropic glutamate receptor selective agonist. *Bioorg Med Chem Lett* **16**:4856-4860.

Springael JY, Urizar E, Costagliola S, Vassart G, and Parmentier M (2007) Allosteric properties of G protein-coupled receptor oligomers. *Pharmacol Ther* **115**:410-418.

Strange PG (2005) Oligomers of D2 dopamine receptors: evidence from ligand binding. *J Mol Neurosci* **26**:155-160.

Suzuki Y, Moriyoshi E, Tsuchiya D, and Jingami H (2004) Negative cooperativity of glutamate binding in the dimeric metabotropic glutamate receptor subtype 1. *J Biol Chem* **279**:35526-35534.

Tateyama M and Kubo Y (2006) Dual signaling is differentially activated by different active states of the metabotropic glutamate receptor 1{alpha}. *Proc Natl Acad Sci U S A* **103**:1124-1128.

Tsuchiya D, Kunishima N, Kamiya N, Jingami H, and Morikawa K (2002) Structural views of the ligand-binding cores of a metabotropic glutamate receptor complexed with an antagonist and both glutamate and Gd3+. *Proc Natl Acad Sci U S A* **99**:2660-2665.

Urizar E, Montanelli L, Loy T, Bonomi M, Swillens S, Gales C, Bouvier M, Smits G, Vassart G, and Costagliola S (2005) Glycoprotein hormone receptors: link between receptor homodimerization and negative cooperativity. *EMBO J* **24**:1954-1964.

Vilardaga JP, Nikolaev VO, Lorenz K, Ferrandon S, Zhuang Z, and Lohse MJ (2008) Conformational cross-talk between alpha(2A)-adrenergic and mu-opioid receptors controls cell signaling. *Nat Chem Biol* **4**:126-131.

White JF, Grodnitzky J, Louis JM, Trinh LB, Shiloach J, Gutierrez J, Northup JK, and Grisshammer R (2007) Dimerization of the class A G protein-coupled neurotensin receptor NTS1 alters G protein interaction. *Proc Natl Acad Sci U S A* **104**:12199-12204.

*Financial Support

This work was supported in part by a research grant from the Ministerio de Educación y Ciencia, Spain (SAF2004-06134).

Send reprint requests to Jesús Giraldo

Grup Biomatemàtic de Recerca, Institut de Neurociències and Unitat de Bioestadística, Universitat Autònoma de Barcelona, 08193 Bellaterra, Spain

E-mail address: Jesus.Giraldo@uab.es

Legends for Figures

Figure 1. The mGlu model. The VFT domain is represented by open-open (OO), open-closed (OC), and closed-closed (CC) dimer states, either free (upper row), singly bound (middle row) or doubly bound (lower row). A conformational induction approach was followed in which the ligand-bound closed states are induced from ligand-bound OO states. For the HD dimer, a two-state model is chosen, with a symmetric arrangement (RR) for the inactive state and an asymmetric structure (RR*) for the active state, and where their relative populations are governed by an equilibrium constant (L). The coupling between VFT and HD is made by allowing the constant L to vary according to the VFT state to which the HD is linked. The equilibrium constants are defined as:

$$2X_1 = \frac{[OC]}{[OO]}; \quad \frac{X_2}{2} = \frac{[CC]}{[OC]}; \quad \frac{K_1}{2} = \frac{[OO][A]}{[O_AO]}; \quad Y_1 = \frac{[O_AC]}{[O_AO]}; \quad Y_2 = \frac{[C_AO]}{[O_AO]};$$

$$Y_3 = \frac{[C_AC]}{[O_AC]}; \quad Y_4 = \frac{[C_AC]}{[C_AO]}; \quad 2K_2 = \frac{[O_AO][A]}{[O_AO_A]}; \quad 2Y_5 = \frac{[O_AC_A]}{[O_AO_A]}; \quad \frac{Y_6}{2} = \frac{[C_AC_A]}{[O_AC_A]}$$

Figure 2. Representation of the fractional binding $f = \frac{[A_{bound}]}{2[R_t]}$ in the absence (solid line) and in the presence of positive (long dashed line) and negative (short dashed line) cooperativity, being x=log[A]. The index of cooperativity is measured by x_d (see Equation A1 in the Appendix), with x_d=0: absence of cooperativity, x_d<0: positive cooperativity; x_d>0: negative cooperativity. In the simulations, x_d=0 (solid curve), x_d=-3 (long dashed curve), and x_d=3 (short dashed curve). The points of inflection are shown as solid circles. One point of inflection (monophasic curve) is found at x=-9 for the absent and positive cooperativity curves, whereas three points of inflection (biphasic curve) are fount at x=-12.3, -9, and -5.7 for the negative cooperativity curve (see Figure 3 for further analysis).

Figure 3. First (f ’, solid lines) and second (f ’’, dashed lines) derivatives of the f(x) function defined by Equation 1, under the conditions used in Figure 2. The index of cooperativity is measured by x_d (see Equation A1 in the Appendix). A point of inflection on the f(x) curve yields a maximum or minimum for f ’(x) and, consequently, a value of 0 for f ’’(x). A. x_d=0 (absence of cooperativity): one inflection point at x=-9. B. x_d=-3 (positive cooperativity): one inflection point at x=-9, C. x_d=3 (negative cooperativity): three inflection points, at -12.3, -9, and -5.7. Inflection points are shown in the Figure as solid circles on f ’(x) and open circles on f ’’(x) (see Figure 2 for the localization of the inflection points on the f(x) function).

Figure 4. Variation of the Hill coefficient at the mid-point (n_{H50}) with the index of cooperativity (x_d) for the binding to the VFT model represented in Figure 1 (Equations A1 and A2); $n_{H50} = 1$ (absence of cooperativity) for x_d=0; $1 < n_{H50} \leq 2$ (positive cooperativity) for x_d<0; and $0 \leq n_{H50} < 1$ (negative cooperativity) for x_d>0. Colors: Green ($1 < n_{H50} \leq 2$ and x_d<0, positive cooperativity and monophasic curve); blue ($0 < n_{H50} < 1$ and 0<x_d≤log2, negative cooperativity and monophasic curve); and red ($0 < n_{H50} < 1$ and x_d>log 2, negative cooperativity and biphasic curve). Solid circle: $n_{H50} = 1$ and x_d=0, absence of cooperativity, monophasic curve.

Figure 5. Comparative modeling of WT and mutated VFT concentration-effect curves (Kniazeff et al., 2004).

A. Experimental data (circles) and simulated empirical Hill equation (Equation 5, line) for the WT mGlu receptor.

B. Experimental data (circles) and mechanistic mGlu model (Equation 2, line) for the WT mGlu receptor. The parameter values for the mechanistic model are listed in Table 3 (best run out of 100 using an evolutionary algorithm).

C. Experimental data (circles) and simulated empirical sum-of-two Hill equations (Equation 6, line) for the single mutated mGlu receptor.

D. Experimental data (circles) and mechanistic mGlu model (Equation 2, line) for the single mutated mGlu receptor. The parameter values for the mechanistic model are listed in Table 3 (best run out of 100 using an evolutionary algorithm).

Figure 6. Distribution of VFT states for WT (A) and mutated (B) receptors (Kniazeff et al., 2004), with the equilibrium constant values taken from Figure 5 mechanistic plots (B and D) and Table 3.

Figure 7. Binding and Induction cooperativities. Conceptual distinction between binding cooperativity (ligand binding to an open state affects the binding of a second ligand) and induction cooperativity (closure of a state affects the closure propensity of the partner if is occupied) allows for different {binding, induction} cooperativity combinations. Two ligands, one showing {negative binding and positive induction} cooperativities (solid line, full agonist) and the other {positive binding and negative induction} cooperativities (dashed line, partial agonist) are shown. Common parameter values: $\alpha_1=10^{-3}$, $\alpha_2=1$, $\alpha_3=10$, $X_1=X_2=10^{-3}$, $Y_1=10^{-4}$. Negative binding and positive induction cooperativities: $K_1=10^{-5}$, $K_2=10^{-3}$, $Y_2=Y_5=10$, $Y_3=Y_6=10^{2}$. Positive binding and negative induction cooperativities: $K_1=10^{-5}$, $K_2=10^{-7}$, $Y_2=Y_5=10$, $Y_3=Y_6=10^{-2}$.

TABLE 1.
Location (x_{50}) and Hill coefficients at the mid-point ($n_{H_{50}}$) of binding curves for glutamate and quisqualate agonists and LY367385 antagonist in the absence and presence of calcium ions (Equations A1 and A2 in the Appendix)

X_1	X_2	K_1	K_2	Y_1	Y_2	Y_3	Y_5	Y_6	x_{50}	$n_{H_{50}}$
Glutamate in the absence of calcium ions										
10^{-4}	10^{-4}	10^{-5}	10^{-2}	10^{-4}	5	10^{3}	5	10^{3}	-5.35 *-5.42*	0.54 *0.55*
Glutamate in the presence of calcium ions										
10^{-4}	10^{-4}	10^{-5}	10^{-2}	10^{-4}	**20**	**$10^{3.8}$**	**20**	**$10^{3.8}$**	-6.05 *-5.89*	0.68 *0.70*
Quisqualate in the absence of calcium ions										
10^{-4}	10^{-4}	10^{-5}	10^{-2}	10^{-4}	10	$10^{4.2}$	10	$10^{4.2}$	-6.1 *-6.34*	1.00 *1.04*
Quisqualate in the presence of calcium ions										
10^{-4}	10^{-4}	10^{-5}	10^{-2}	10^{-4}	**30**	**$10^{4.4}$**	**30**	**$10^{4.4}$**	-6.44 *-6.68*	0.90 *0.92*
Antagonist (LY367385) in the absence of calcium ions										
10^{-4}	10^{-4}	10^{-6}	10^{-6}	10^{-4}	10^{-4}	10^{-4}	10^{-4}	10^{-4}	-6.00 *-6.05*	1.00 *1.06*
Antagonist (LY367385) in the presence of calcium ions										
10^{-4}	10^{-4}	10^{-6}	10^{-6}	10^{-4}	**10^{-2}**	**10^{-2}**	**10^{-2}**	**10^{-2}**	-6.00 *-5.92*	1.00 *0.92*

In bold, the values of the parameters that are changed in the model upon addition of calcium. Pharmacologic curve-shape descriptors, x_{50} and $n_{H_{50}}$: In roman, calculated values; in italics, experimental values (Suzuki et al., 2004). In the experiments, glutamate shows negative cooperativity ($n_{H_{50}} < 1$). Calcium effect is agonist-dependent: Calcium decreases the x_{50} values for the agonists but not for the antagonist; in addition, calcium increases the Hill coefficient of glutamate binding. In the mechanistic model, negative binding cooperativity ($K_1<K_2$) and positive induction cooperativity ($Y_2<Y_3$; $Y_5<Y_6$) was assumed for the agonists whereas absence of cooperativity was assumed for the antagonist.

The Y_4 equilibrium constant (see Figure 1) has not been included explicitly in the Table because is automatically determined by the values of Y_1, Y_2 and Y_3 (see main text).

TABLE 2.
Variation of the parameters included in the definition of Basal and Maximum responses (Equations 3 and 4)

X_1	X_2	Y_5	Y_6	L_1	L_2	L_3	Basal response	Maximum response	$\log \frac{\text{Maximum}}{\text{Basal}}$
Positive agonists									
10^{-4}	10^{-1}	1	10^{2}	10^{-4}	1	10^{2}	$2.6\ 10^{-3}$	0.99	2.6
10^{-4}	10^{-1}	$\mathbf{10^{-4}}$	10^{2}	10^{-4}	1	10^{2}	$2.6\ 10^{-3}$	0.66	2.4
10^{-4}	10^{-1}	1	$\mathbf{10^{-1}}$	10^{-4}	1	10^{2}	$2.6\ 10^{-3}$	0.89	2.5
10^{-4}	10^{-1}	$\mathbf{10^{-1}}$	$\mathbf{10^{-1}}$	10^{-4}	1	10^{2}	$2.6\ 10^{-3}$	0.66	2.4
Inverse agonists									
10^{-4}	10^{-1}	$\mathbf{10^{-5}}$	$\mathbf{10^{-1}}$	10^{-4}	1	10^{2}	$2.6\ 10^{-3}$	$4.4\ 10^{-4}$	-0.8
10^{-4}	10^{-1}	$\mathbf{10^{-4}}$	$\mathbf{10^{-2}}$	10^{-4}	1	10^{2}	$2.6\ 10^{-3}$	$8.0\ 10^{-4}$	-0.5
10^{-4}	10^{-1}	$\mathbf{10^{-5}}$	$\mathbf{10^{-2}}$	10^{-4}	1	10^{2}	$2.6\ 10^{-3}$	$2.6\ 10^{-4}$	-1.0

In bold, the parameters changed relative to a reference state (upper row). Lowering either/both Y_5 or/and Y_6 decreases the maximum response, leading to partial agonism. Decreasing Y_5 and/or Y_6 below the values in the absence of ligand (X_1 and X_2, respectively) leads to inverse agonism ($\log(\text{Maximum/Basal})<0$). Note that for an inverse agonist Maximum should read as Minimum.

TABLE 3.
Interpretation of the experimental functional data included in Kniazeff et al., 2004 under the mGlu model depicted in Equation 2

WT

Mechanistic parameters

	X_1	X_2	K_1	K_2	Y_1	Y_2	Y_3	Y_5	Y_6	L_1	L_2	L_3
Mean ±SD	-5.07 ±1.90	-4.30 ±1.50	-6.02 ±0.08	-4.07 ±0.82	-4.56 ±1.50	0.84 ±0.76	1.52 ±0.97	-0.01 ±0.69	2.79 ±0.86	-0.37 ±0.02	-0.21 ±0.57	1.81 ±0.35
Best run	-6.23	-3.70	-6.10	-3.46	-5.03	0.63	1.15	0.00	3.45	-0.37	0.02	1.55

Pharmacologic curve-shape descriptors

	Basal response	Maximum response	x_{50}	n_{H50}	x_I
Empirical	*0.46*	*0.99*	*-7.24*	*1.26*	*-7.24*
Best run	0.46	0.99	-7.24	1.33	-7.25

Single Mutated VFT

Mechanistic parameters

	X_1	X_2	K_1	K_2	Y_1	Y_2	Y_3	Y_5	Y_6	L_1	L_2	L_3
Mean ±SD	-6.85* ±1.24	-5.95* ±1.56	-5.90 ±0.36	-2.41* ±0.54	-4.63 ±1.49	0.42* ±0.51	1.30 ±1.16	0.03 ±0.46	1.28* ±0.49	-0.47* ±0.00	-0.17 ±0.20	0.71* ±0.09
Best run	-6.92	-5.92	-6.16	-2.27	-3.95	0.12	1.60	0.31	0.88	-0.47	-0.09	0.72

Pharmacologic curve-shape descriptors

	Basal response	Maximum response	x_{50}	n_{H50}	x_{I1}	x_{I2}	x_{I3}
Empirical	*0.41*	*0.89*	*-3.92*	*0.62*	*-6.92*	*-5.49*	*-3.55*
Best run	0.40	0.89	-3.94	0.57	-6.94	-5.44	-3.53

Equilibrium constants are expressed in logarithmic form. An in-house evolutionary algorithm was used for parameter optimization (see Methods). 100 independents runs were performed for both WT and mutated receptors; Mean and SD are shown; the best (closest to the mean parameters) run is also shown. The parameter values for the latter run were used for graphic representation in Figure 5.

Statistical comparison between WT and mutated receptor samples for each of the parameters was done by Student's t-test including Sidàk correction for multiple testing, *P<0.05.

Pharmacologic curve-shape descriptors, Basal and Maximum responses, location (x_{50}), Hill coefficient at the mid-point (n_{H50}) and point(s) of inflection (x_I), are shown. Italic and Roman characters for empirical and mechanistic equations, respectively, were used.

The Y_4 equilibrium constant (see Figure 1) has not been included explicitly in the Table because is automatically determined by the values of Y_1, Y_2 and Y_3 (see main text).

TABLE 4.
Association of the mechanistic parameters of the model with typical pharmacological properties of the functional response (see also the simulations in the Supplementary material)

Pharmacologic properties of the functional response	**Mechanistic parameters**[1]
Basal response $\frac{1}{1+\frac{1}{2}\cdot\frac{1+2X_1+X_1X_2}{L_1+2L_2X_1+L_3X_1X_2}}$	X_1, X_2 (VFT) L_1, L_2, L_3 (HD) Increasing the receptor parameters increases the basal response of the mutant receptor relative to the WT (it is assumed that $L_1<L_2<L_3$).
Efficacy $\frac{1}{1+\frac{1}{2}\cdot\frac{1+2Y_5+Y_5Y_6}{L_1+2L_2Y_5+L_3Y_5Y_6}}$	Y_5, Y_6 (VFT) Increasing Y_5 and Y_6 (the constants inducing closed states in the doubly occupied receptor) increases the efficacy of the ligand (it is assumed that the L constants are independent of the ligand). A full agonist results from high Y_5 and Y_6 whereas a partial agonist can be obtained by decreasing Y_6 relative to Y_5. An inverse agonist can be obtained by decreasing Y_5 and Y_6 relative to X_1 and X_2.
[2]*Potency* (A_{50}) $\frac{-b\pm\sqrt{b^2-4ac}}{2a}$	K_1, K_2, Y_1 to Y_6 (VFT) The potency of the agonist depends on both the affinity constants to the open states (K_1, K_2) and the induction constants of closed states (Y_1 to Y_6). A parallel displacement to the left or the right results by simultaneous decrease or increase of K_1 and K_2, respectively.
Biphasic and bell-shaped curves	K_1, K_2, Y_1 to Y_6 (VFT) Biphasic curves can be obtained by different ways: Increasing K_2 (reducing the affinity of the second ligand for the OO state); increasing Y_2 and Y_3 (increasing the capacity to induce closed states in the singly occupied receptor); decreasing Y_5 (reducing the ability to induce the CO state in the doubly occupied receptor) or both Y_5 and Y_6 (reducing the ability to induce the CC state in the doubly occupied receptor). Relative very low values of Y_5 and Y_6 may produce a bell-shaped curve.

[1]See Figure 1.
[2]See Equation A9 in the Appendix for definition of the parameters of the equation.

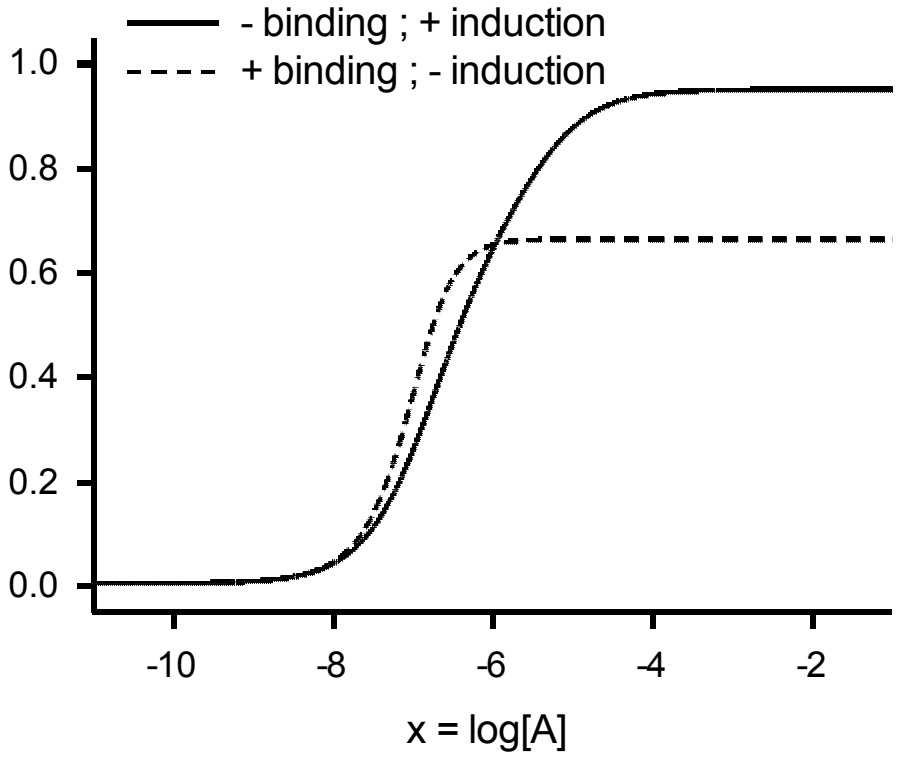
- binding ; + induction
+ binding ; - induction
1.0
0.8
0.6
0.4
0.2
0.0
-10
-8
-6
-4
-2
x = log[A]

Figure 7

FIGURE 1

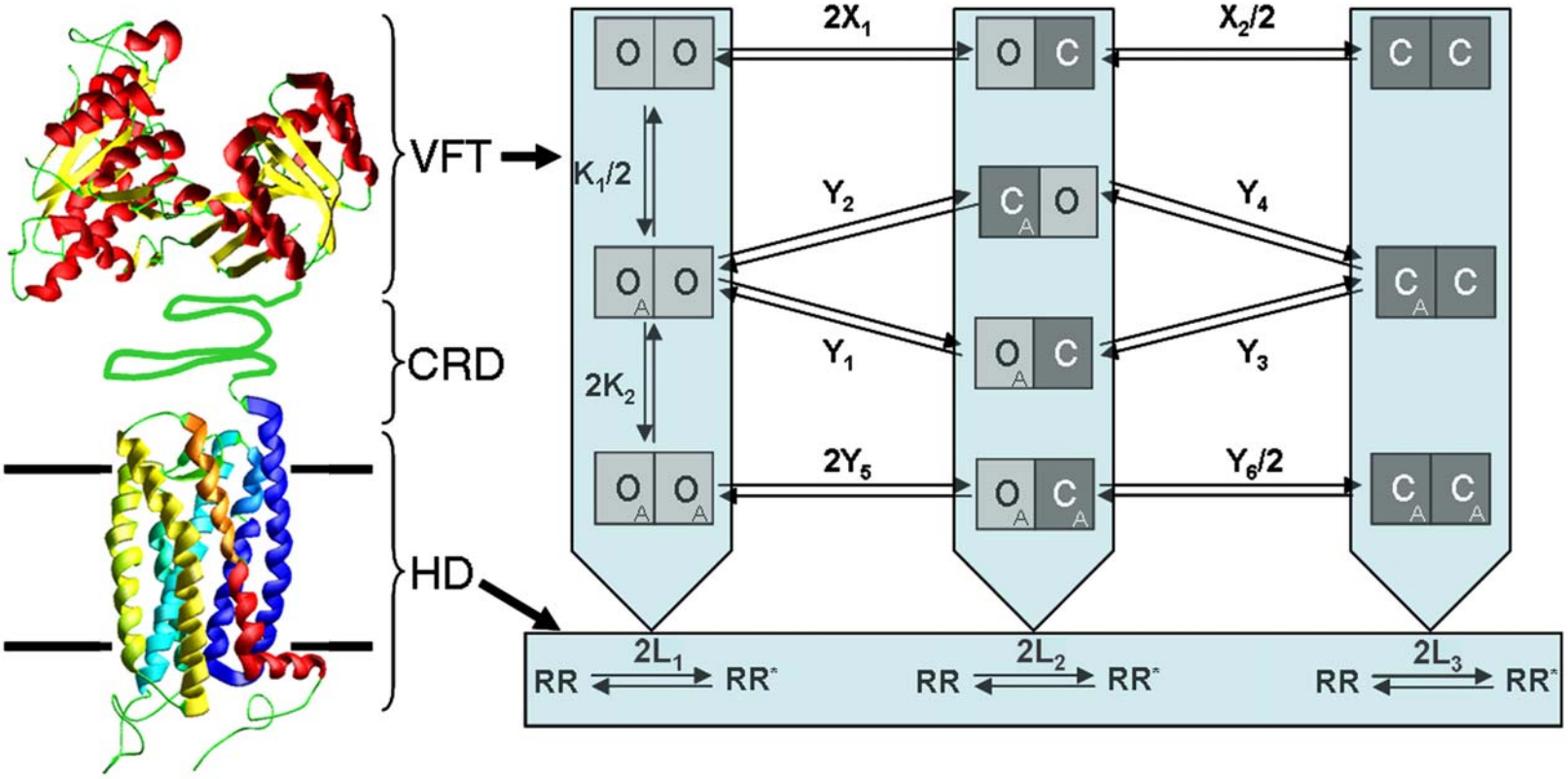
VFT
CRD
HD
O O
O C
C C
C O
O O
O C
C C
O O
O C
C C
2X1
X2/2
K1/2
Y2
Y4
Y1
Y3
2K2
2Y5
Y6/2
2L1
2L2
2L3
RR
RR*
RR
RR*
RR
RR*

FIGURE 2

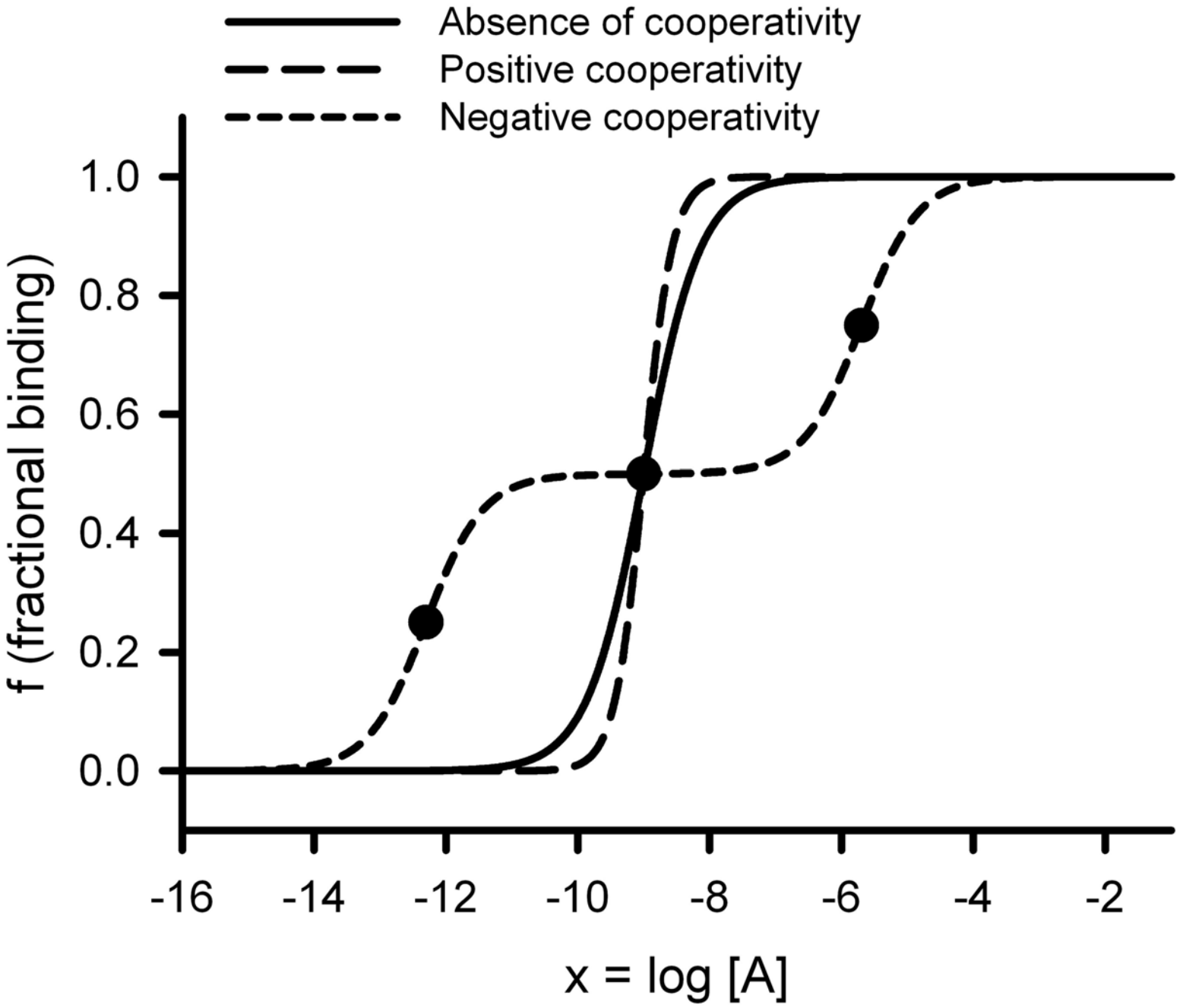
Absence of cooperativity
Positive cooperativity
Negative cooperativity
1.0
0.8
0.6
0.4
0.2
0.0
f (fractional binding)
-16
-14
-12
-10
-8
-6
-4
-2
x = log [A]

FIGURE 3

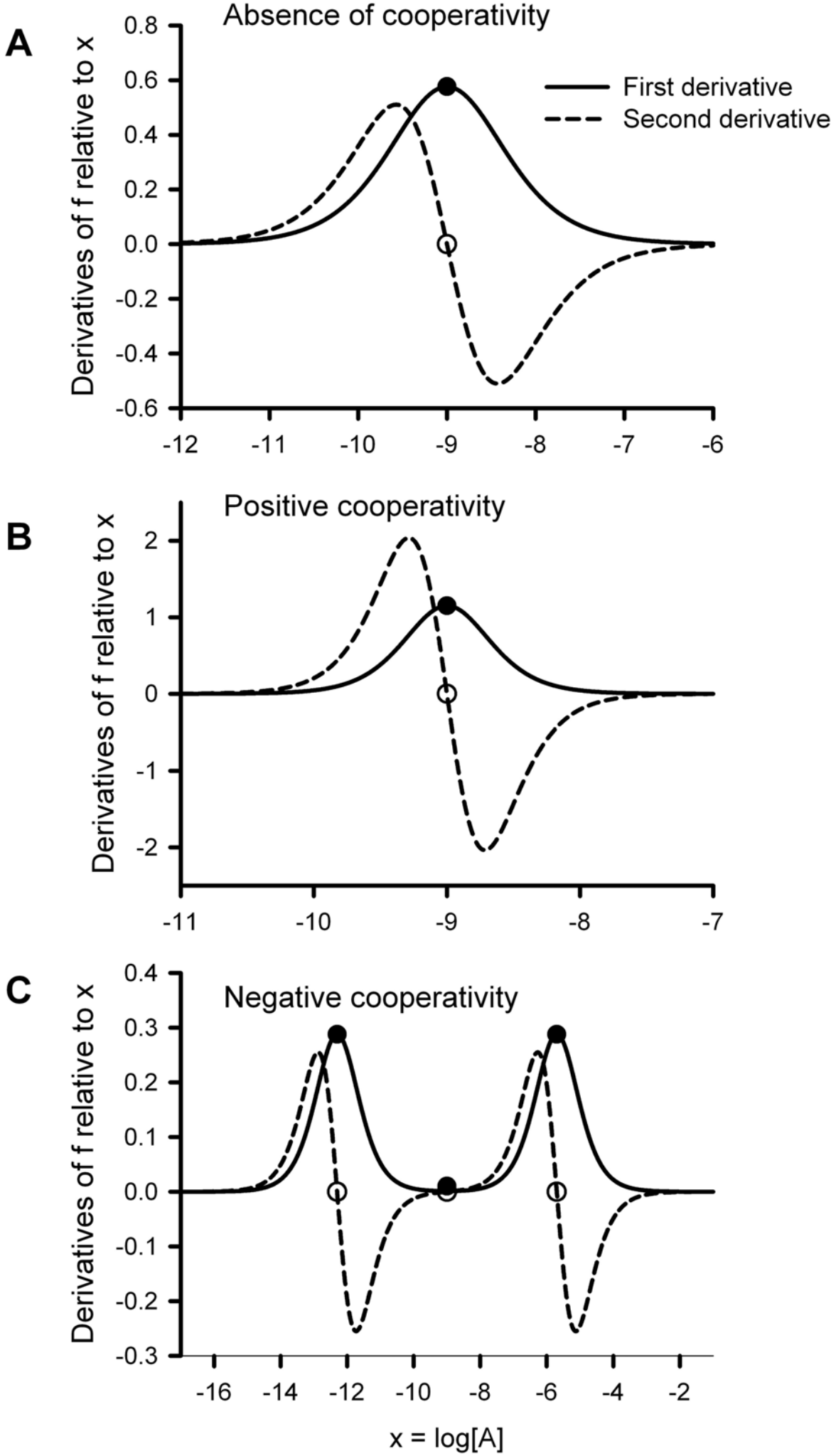
A
Absence of cooperativity
Derivatives of f relative to x
First derivative
Second derivative
0.8
0.6
0.4
0.2
0.0
-0.2
-0.4
-0.6
-12
-11
-10
-9
-8
-7
-6
B
Positive cooperativity
Derivatives of f relative to x
2
1
0
-1
-2
-11
-10
-9
-8
-7
C
Negative cooperativity
Derivatives of f relative to x
0.4
0.3
0.2
0.1
0.0
-0.1
-0.2
-0.3
-16
-14
-12
-10
-8
-6
-4
-2
x = log[A]

FIGURE 4

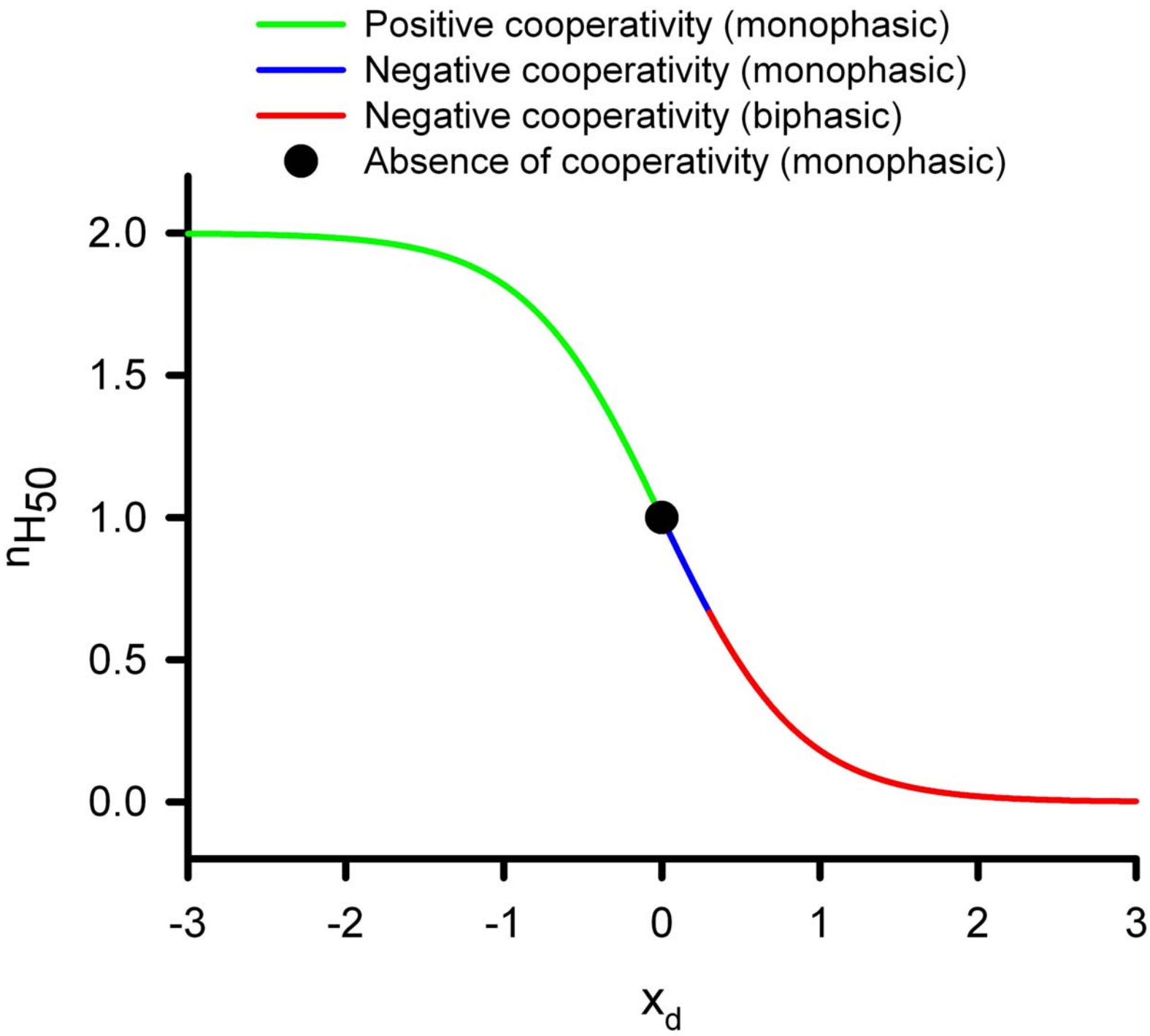
Positive cooperativity (monophasic)
Negative cooperativity (monophasic)
Negative cooperativity (biphasic)
Absence of cooperativity (monophasic)
2.0
1.5
1.0
0.5
0.0
n_{H50}
-3
-2
-1
0
1
2
3
x_d

FIGURE 5

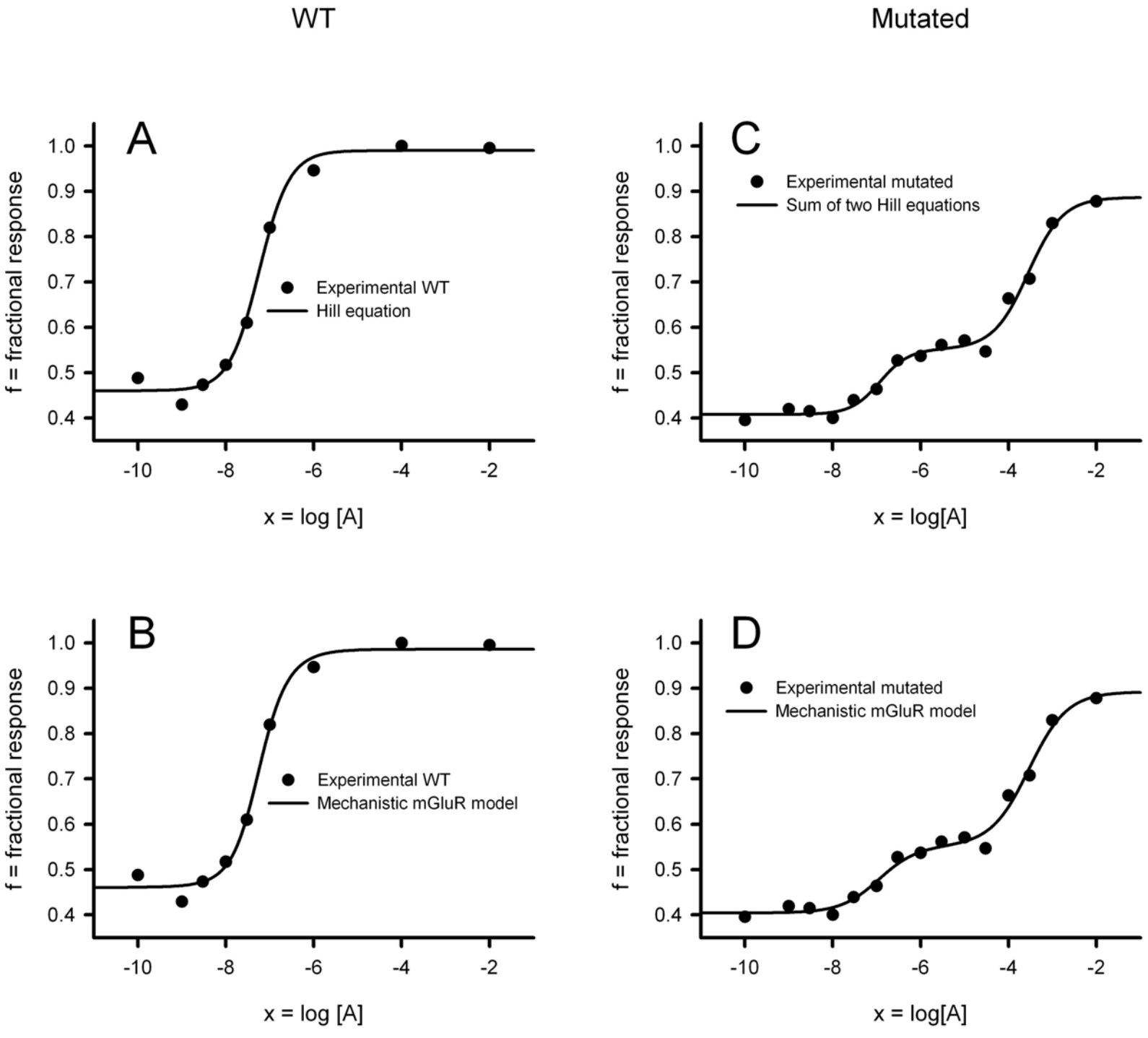
WT
Mutated
A
B
C
D
f = fractional response
x = log [A]
x = log[A]
Experimental WT
Hill equation
Experimental WT
Mechanistic mGluR model
Experimental mutated
Sum of two Hill equations
Experimental mutated
Mechanistic mGluR model
1.0
0.9
0.8
0.7
0.6
0.5
0.4
-10
-8
-6
-4
-2

FIGURE 6

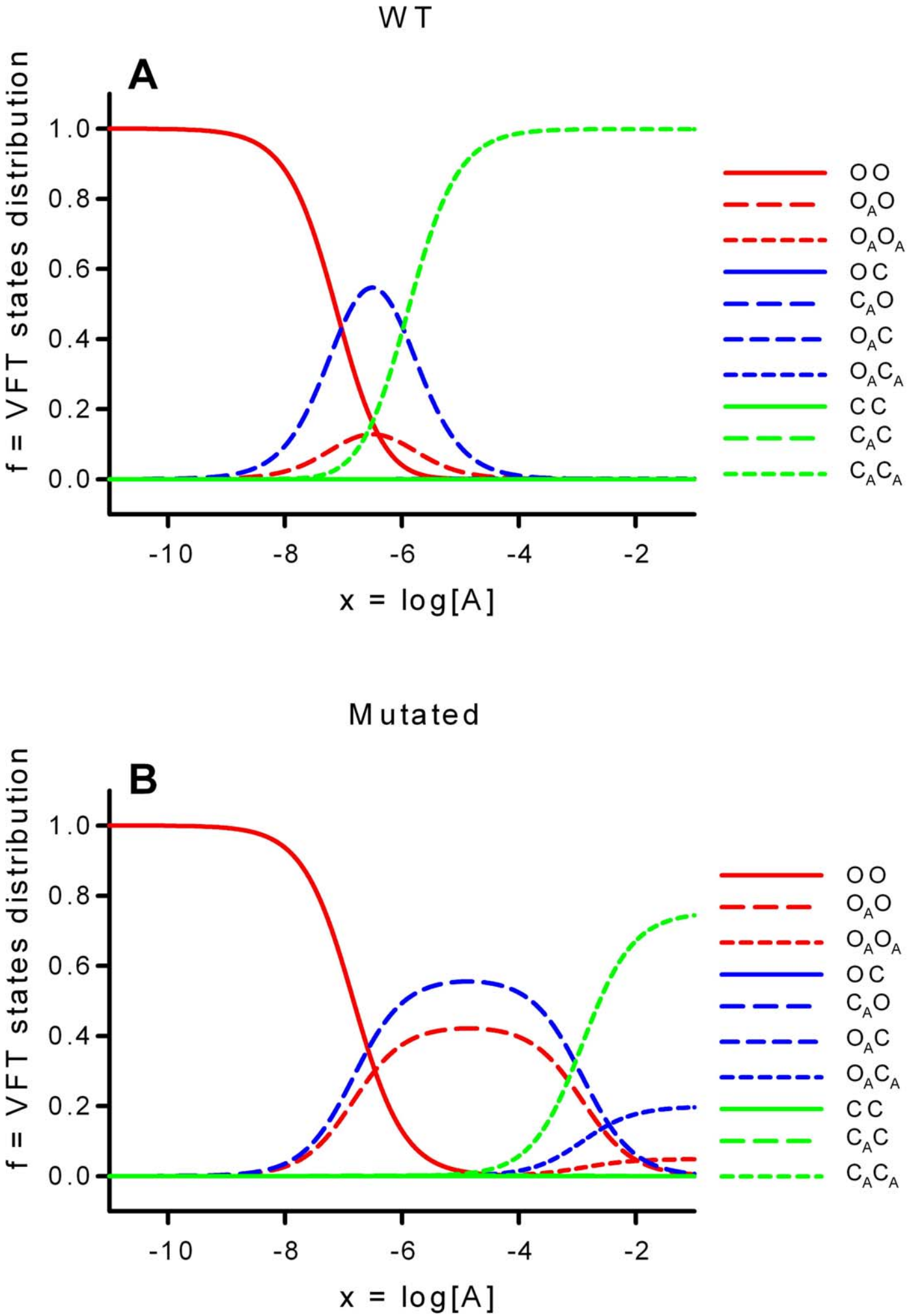
WT
A
f = VFT states distribution
1.0
0.8
0.6
0.4
0.2
0.0
-10
-8
-6
-4
-2
x = log[A]
OO
OAO
OAOA
OC
CAO
OAC
OACA
CC
CAC
CACA
Mutated
B
f = VFT states distribution
1.0
0.8
0.6
0.4
0.2
0.0
-10
-8
-6
-4
-2
x = log[A]
OO
OAO
OAOA
OC
CAO
OAC
OACA
CC
CAC
CACA